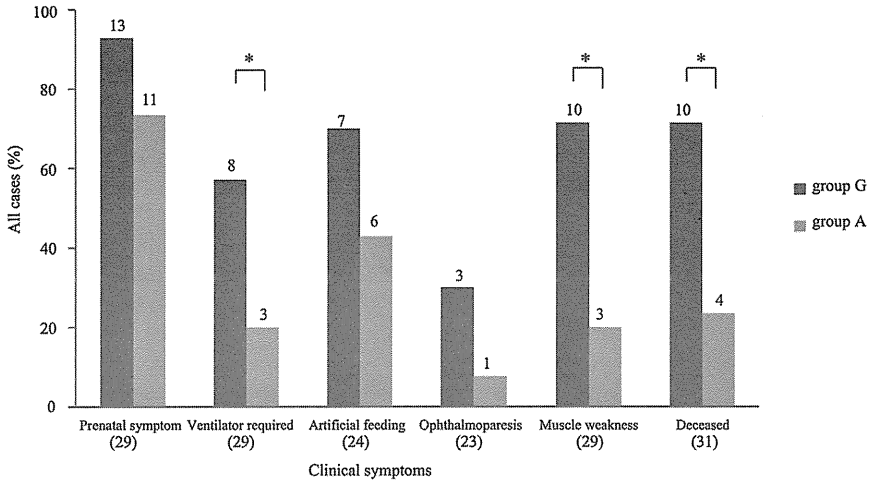

Figure 5. Correlation between the c.1582G>A (p.Glu528Lys) Mutation and Clinical Features

The clinical characteristics of NEM are shown for the two groups of affected individuals (32 total), either with the c.1582G>A (p.Glu528Lys) mutation (as group A) or without it (as group G). The numbers of total affected individuals with clinical records regarding either the presence or the absence of each characteristic are indicated below the bars, and the numbers of affected individuals in each group are indicated above the respective bars. Labels on the x axis are as follows: prenatal symptoms, individuals demonstrating either fetal akinesia or hypokinesia, polyhydramnios, or fetal edema or effusion; ventilator required, individuals with respiratory failure requiring ventilation; artificial feeding, dysphagia-affected persons requiring tube feeding or gastrostomy; ophthalmoparesis, individuals with ophthalmoparesis along with facial weakness; muscle weakness, individuals with the most severe form of muscle weakness and demonstrating no antigravitory movement; and deceased, individuals who were deceased at the time of study. Asterisks indicate that statistical significance was observed.

odds ratio = 8.125; 95% confidence interval = 1.62–40.75) (Figure 5). We further compared the clinical features of individuals of different ethnicities (either European or Asian descent) according to the c.1582G>A genotype, and similar tendencies were demonstrated (data not shown). There was, however, great variation in severity for individuals with or without the c.1582G>A genotype.

Discussion

We have described the identification of recessive *KLHL40* mutations in individuals with severe NEM from 28 unrelated families of various ethnicities. The c.1582G>A mutation was the most frequently detected mutation and was found in Japanese, Kurdish, and Turkish persons. However, comparison of haplotypes between a Japanese family and a Turkish family suggested that the mutation arose independently in these ethnic groups. We have shown several lines of evidence of the pathogenicity of the *KLHL40* mutations. The missense mutations occurred mostly in conserved functional domains within KLHL40, and they were predicted to destabilize the intramolecular interactions and thus impair protein stability. This was corroborated by the absence of KLHL40 even in the skeletal muscle of individuals harboring two missense mutations. We have established a locus-specific database for *KLHL40* mutations at the Leiden Muscular Dystrophy Pages.

Expression of KLHL40 in fetal and adult skeletal muscle indicates that KLHL40 plays a role in both myogenesis and mature muscle. KLHL40 appears to be more abundant in fetal skeletal muscle than in postnatal skeletal muscle and most likely accounts for the prevalence of in utero presentations in this NEM cohort. Perhaps KLHL40 is more important for myogenesis than for muscle maintenance; this could account for the fact that the disease ranges so much in severity, from some individuals' dying within hours of being born to others' surviving into adolescence. Our zebrafish studies have demonstrated that Klhl40a and Klhl40b are not required for the specification of muscle cells but rather for muscle patterning and function and that loss of either isoform in the early embryo is sufficient to impair normal mobility, supporting the involvement of KLHL40 in NEM-associated fetal akinesia. It has previously been suggested that KLHL40 is also important for muscle maintenance through the process of degeneration and regeneration.[29,30] *Klhl40* is upregulated in myogenic precursors after cardiotoxin injury of mouse skeletal muscle, supporting a role for *Klhl40* in the response to muscle damage.[29] Studies of cattle muscle have shown increased *Klhl40* expression in another catabolic process, undernutrition, further suggesting a role for *KLHL40* in the stress response.[30]

KLHL40 belongs to the superfamily of kelch-repeat-containing proteins that form characteristic β-propeller structures,[31] which bind substrate proteins and are involved in a wide variety of functions. In humans, 71 kelch-repeat-containing proteins have been identified.[31] The majority contain an N-terminal BTB domain (also known as the POZ [poxvirus and zinc finger] domain) and a BACK motif. Proteins containing both a BTB domain and a kelch repeat have previously been implicated in neuromuscular disease. A dominant *KLHL9* mutation causes an early-onset distal myopathy (distal myopathy 1 [MIM 160500]),[32] and dominant *KBTBD13* mutations cause nemaline myopathy with cores (MIM 609273).[9] We now show that *KLHL40*, encoding KLHL40, which contains both a BTB domain and a kelch repeat, is associated with autosomal-recessive neuromuscular disease. BTB domains function as substrate-specific adaptors for cullin 3 (Cul3),[33,34] a component of the E3-ubiquitin-ligase complex. Both KLHL9 and KBTBD13 bind Cul3.[10,32] MuRF1,

an E3-ubiquitin ligase, is known to be recruited to M-line titin and is thought to modulate myofibrillar turnover and the trophic state of muscle.[35] KLHL40 appears to be present at the A-band and might be similarly involved through the ubiquitin-proteasome pathway.

We have characterized the severe and distinctive features of this disease as fetal akinesia or hypokinesia during the prenatal period, respiratory failure and swallowing difficulty at birth, contractures and fractures along with dysmorphic features, and in most cases, early death. We have also shown that persons with the recurrent c.1582G>A mutation tend to have relatively milder symptoms compared to those of individuals without c.1582G>A. However, the severity of the disease in persons with or without the c.1582G>A genotype varied greatly (for example, from death at 20 days to still being alive at 11 years for persons homozygous for the c.1582G>A genotype), suggesting modifying factors.

Fetal akinesias are clinically and genetically heterogeneous, and the majority of cases still remain genetically unsolved.[36] Primary muscle diseases account for up to 50% of such syndromes.[37] On the basis of our study, *KLHL40* mutations cause a significant proportion of severe NEM cases of fetal akinesia sequence and the disease shows worldwide prevalence. *KLHL40* should be considered when a clinician encounters an individual presenting with prenatal symptoms, such as fetal akinesia or hypokinesia, or clinical features and/or pathology of severe NEM at birth (especially miliary NEM, which was present in at least 20% of our *KLHL40*-mutation cases), along with an autosomal-recessive pattern of family history. Fractures are a relatively frequent presentation within this cohort, unlike other NEM cohorts, and should also be used for directing genetic screening of *KLHL40*. We show that KLHL40 immunohistochemistry, immunoblotting, or genetic screening will identify the disease and thus allow genetic counseling for the affected individual's family.

In conclusion, this study associates loss-of-function *KLHL40* mutations with severe, often in utero, NEM. Many probands who do not harbor *KLHL40* mutations present with NEM in utero, suggesting further genetic heterogeneity. Clarification of KLHL40 function and interactions might lead to a greater understanding of the pathogenesis of disease, the identification of other candidates for this severe form of NEM, and the investigation of possible therapies.

Supplemental Data

Supplemental Data include 11 figures, three tables, and two movies and can be found with this article online at http://www.cell.com/AJHG.

Acknowledgments

This research was supported by the National Health and Medical Research Council of Australia (fellowships APP1035955 to G.R. and APP1002147 to N.G.L. and grant APP1022707) and Association Francaise contre les Myopathies (AFM; AFM15734). E.T. and K.S.Y. are supported by university postgraduate awards. This work received grants from the Ministry of Health, Labour, and Welfare (N. Miyake, H.S., and N. Matsumoto), Japan Science and Technology Agency (N. Matsumoto), Strategic Research Program for Brain Sciences (E.K. and N. Matsumoto), and Takeda Science Foundation (N. Miyake and N. Matsumoto) and Grants-in-Aid for Scientific Research on Innovative Areas (Transcription Cycle) from the Ministry of Education, Culture, Sports, Science, and Technology of Japan (N. Miyake and N. Matsumoto) and for Scientific Research from the Japan Society for the Promotion of Science (N. Miyake, H.S., and N. Matsumoto). The A.H.B. laboratory was supported by the National Institutes of Health (R01-AR044345) and the Muscular Dystrophy Association (MDA201302). O.C. is a Dubai Harvard Foundation for Medical Research Fellow and a grantee of the Schlumberger Foundation Faculty for the Future Program. E.B. is supported by grants from Telethon (GUP08005) and the Ministry of Health on Congenital Myopathies. F.M. is supported by the Great Ormond Street Children's Charity and National Specialist Commissioning Group. P.V. and V.-L.L. were supported by grants to C.W.-P. by the AFM, Sigrid Jusélius Foundation, Academy of Finland, Finska Läkaresällskapet, and Medicinska Understödsföreningen Liv och Hälsa r.f. R.V. is supported by a Monash Graduate Research Scholarship and a Faculty of Science Dean's International Postgraduate Research Scholarship.

Received: March 15, 2013
Revised: April 25, 2013
Accepted: May 3, 2013
Published: June 6, 2013

Web Resources

The URLs for data presented herein are as follows:

1000 Genomes Project, http://www.1000genomes.org/
dbSNP, http://www.ncbi.nlm.nih.gov/projects/SNP/
Leiden Open Variation Database, www.LOVD.nl/KLHL40
NHLBI Exome Sequencing Project (ESP) Exome Variant Server, http://evs.gs.washington.edu/EVS/
Online Mendelian Inheritance in Man (OMIM), http://www.omim.org
PyMOL, http://www.pymol.org
RefSeq, http://www.ncbi.nlm.nih.gov/RefSeq

References

1. Nance, J.R., Dowling, J.J., Gibbs, E.M., and Bönnemann, C.G. (2012). Congenital myopathies: an update. Curr. Neurol. Neurosci. Rep. *12*, 165–174.
2. Nowak, K.J., Davis, M.R., Wallgren-Pettersson, C., Lamont, P.J., and Laing, N.G. (2012). Clinical utility gene card for: nemaline myopathy. Eur. J. Hum. Genet. *20*. Published online April 18, 2012. http://dx.doi.org/10.1038/ejhg.2012.70.
3. Nowak, K.J., Wattanasirichaigoon, D., Goebel, H.H., Wilce, M., Pelin, K., Donner, K., Jacob, R.L., Hübner, C., Oexle, K., Anderson, J.R., et al. (1999). Mutations in the skeletal muscle alpha-actin gene in patients with actin myopathy and nemaline myopathy. Nat. Genet. *23*, 208–212.
4. Agrawal, P.B., Greenleaf, R.S., Tomczak, K.K., Lehtokari, V.L., Wallgren-Pettersson, C., Wallefeld, W., Laing, N.G., Darras,

B.T., Maciver, S.K., Dormitzer, P.R., and Beggs, A.H. (2007). Nemaline myopathy with minicores caused by mutation of the CFL2 gene encoding the skeletal muscle actin-binding protein, cofilin-2. Am. J. Hum. Genet. *80*, 162–167.

5. Lehtokari, V.L., Pelin, K., Sandbacka, M., Ranta, S., Donner, K., Muntoni, F., Sewry, C., Angelini, C., Bushby, K., Van den Bergh, P., et al. (2006). Identification of 45 novel mutations in the nebulin gene associated with autosomal recessive nemaline myopathy. Hum. Mutat. *27*, 946–956.
6. Johnston, J.J., Kelley, R.I., Crawford, T.O., Morton, D.H., Agarwala, R., Koch, T., Schäffer, A.A., Francomano, C.A., and Biesecker, L.G. (2000). A novel nemaline myopathy in the Amish caused by a mutation in troponin T1. Am. J. Hum. Genet. *67*, 814–821.
7. Donner, K., Ollikainen, M., Ridanpää, M., Christen, H.J., Goebel, H.H., de Visser, M., Pelin, K., and Wallgren-Pettersson, C. (2002). Mutations in the beta-tropomyosin (TPM2) gene—a rare cause of nemaline myopathy. Neuromuscul. Disord. *12*, 151–158.
8. Laing, N.G., Wilton, S.D., Akkari, P.A., Dorosz, S., Boundy, K., Kneebone, C., Blumbergs, P., White, S., Watkins, H., Love, D.R., et al. (1995). A mutation in the alpha tropomyosin gene TPM3 associated with autosomal dominant nemaline myopathy. Nat. Genet. *9*, 75–79.
9. Sambuughin, N., Yau, K.S., Olivé, M., Duff, R.M., Bayarsaikhan, M., Lu, S., Gonzalez-Mera, L., Sivadorai, P., Nowak, K.J., Ravenscroft, G., et al. (2010). Dominant mutations in KBTBD13, a member of the BTB/Kelch family, cause nemaline myopathy with cores. Am. J. Hum. Genet. *87*, 842–847.
10. Sambuughin, N., Swietnicki, W., Techtmann, S., Matrosova, V., Wallace, T., Goldfarb, L., and Maynard, E. (2012). KBTBD13 interacts with Cullin 3 to form a functional ubiquitin ligase. Biochem. Biophys. Res. Commun. *421*, 743–749.
11. Lammens, M., Moerman, P., Fryns, J.P., Lemmens, F., van de Kamp, G.M., Goemans, N., and Dom, R. (1997). Fetal akinesia sequence caused by nemaline myopathy. Neuropediatrics *28*, 116–119.
12. Lacson, A.G., Donaldson, G., Barness, E.G., Ranells, J.D., and Pomerance, H.H. (2002). Infant with high arched palate, bell-shaped chest, joint contractures, and intrauterine fractures. Pediatr. Pathol. Mol. Med. *21*, 569–584.
13. Ravenscroft, G., Jackaman, C., Bringans, S., Papadimitriou, J.M., Griffiths, L.M., McNamara, E., Bakker, A.J., Davies, K.E., Laing, N.G., and Nowak, K.J. (2011). Mouse models of dominant ACTA1 disease recapitulate human disease and provide insight into therapies. Brain *134*, 1101–1115.
14. Abecasis, G.R., Cherny, S.S., Cookson, W.O., and Cardon, L.R. (2002). Merlin—rapid analysis of dense genetic maps using sparse gene flow trees. Nat. Genet. *30*, 97–101.
15. Ravenscroft, G., Thompson, E.M., Todd, E.J., Yau, K.S., Kresoje, N., Sivadorai, P., Friend, K., Riley, K., Manton, N.D., Blumbergs, P., et al. (2013). Whole exome sequencing in foetal akinesia expands the genotype-phenotype spectrum of GBE1 glycogen storage disease mutations. Neuromuscul. Disord. *23*, 165–169.
16. Wang, K., Li, M., and Hakonarson, H. (2010). ANNOVAR: functional annotation of genetic variants from high-throughput sequencing data. Nucleic Acids Res. *38*, e164.
17. Harrow, J., Denoeud, F., Frankish, A., Reymond, A., Chen, C.K., Chrast, J., Lagarde, J., Gilbert, J.G., Storey, R., Swarbreck, D., et al. (2006). GENCODE: producing a reference annotation for ENCODE. Genome Biol. *7*(*Suppl 1*), S4.1–S4.9.
18. Garritano, S., Gemignani, F., Voegele, C., Nguyen-Dumont, T., Le Calvez-Kelm, F., De Silva, D., Lesueur, F., Landi, S., and Tavtigian, S.V. (2009). Determining the effectiveness of High Resolution Melting analysis for SNP genotyping and mutation scanning at the TP53 locus. BMC Genet. *10*, 5.
19. Doi, H., Yoshida, K., Yasuda, T., Fukuda, M., Fukuda, Y., Morita, H., Ikeda, S., Kato, R., Tsurusaki, Y., Miyake, N., et al. (2011). Exome sequencing reveals a homozygous SYT14 mutation in adult-onset, autosomal-recessive spinocerebellar ataxia with psychomotor retardation. Am. J. Hum. Genet. *89*, 320–327.
20. Schymkowitz, J., Borg, J., Stricher, F., Nys, R., Rousseau, F., and Serrano, L. (2005). The FoldX web server: an online force field. Nucleic Acids Res. *33*(Web Server issue), W382–W388.
21. Van Durme, J., Delgado, J., Stricher, F., Serrano, L., Schymkowitz, J., and Rousseau, F. (2011). A graphical interface for the FoldX forcefield. Bioinformatics *27*, 1711–1712.
22. Nowak, K.J., Ravenscroft, G., Jackaman, C., Filipovska, A., Davies, S.M., Lim, E.M., Squire, S.E., Potter, A.C., Baker, E., Clément, S., et al. (2009). Rescue of skeletal muscle alpha-actin-null mice by cardiac (fetal) alpha-actin. J. Cell Biol. *185*, 903–915.
23. Ravenscroft, G., Nowak, K.J., Jackaman, C., Clément, S., Lyons, M.A., Gallagher, S., Bakker, A.J., and Laing, N.G. (2007). Dissociated flexor digitorum brevis myofiber culture system—a more mature muscle culture system. Cell Motil. Cytoskeleton *64*, 727–738.
24. Ruparelia, A.A., Zhao, M., Currie, P.D., and Bryson-Richardson, R.J. (2012). Characterization and investigation of zebrafish models of filamin-related myofibrillar myopathy. Hum. Mol. Genet. *21*, 4073–4083.
25. Zeller, J., Schneider, V., Malayaman, S., Higashijima, S., Okamoto, H., Gui, J., Lin, S., and Granato, M. (2002). Migration of zebrafish spinal motor nerves into the periphery requires multiple myotome-derived cues. Dev. Biol. *252*, 241–256.
26. Abecasis, G.R., Auton, A., Brooks, L.D., DePristo, M.A., Durbin, R.M., Handsaker, R.E., Kang, H.M., Marth, G.T., and McVean, G.A.; 1000 Genomes Project Consortium. (2012). An integrated map of genetic variation from 1,092 human genomes. Nature *491*, 56–65.
27. Kimura, M., and Ota, T. (1973). The age of a neutral mutant persisting in a finite population. Genetics *75*, 199–212.
28. Guerois, R., Nielsen, J.E., and Serrano, L. (2002). Predicting changes in the stability of proteins and protein complexes: a study of more than 1000 mutations. J. Mol. Biol. *320*, 369–387.
29. Embree, E.J. (2007). The identification and characterization of MKRP, a novel kelch related protein. PhD Thesis, Graduate School of Biomedical Sciences, The University of Texas Southwestern Medical Center at Dallas, Dallas, TX. http://repositories.tdl.org/utswmed-ir/bitstream/handle/2152.5/226/embreelaurence.pdf?sequence=3.
30. Lehnert, S.A., Byrne, K.A., Reverter, A., Nattrass, G.S., Greenwood, P.L., Wang, Y.H., Hudson, N.J., and Harper, G.S. (2006). Gene expression profiling of bovine skeletal muscle in response to and during recovery from chronic and severe undernutrition. J. Anim. Sci. *84*, 3239–3250.
31. Prag, S., and Adams, J.C. (2003). Molecular phylogeny of the kelch-repeat superfamily reveals an expansion of BTB/kelch proteins in animals. BMC Bioinformatics *4*, 42.
32. Cirak, S., von Deimling, F., Sachdev, S., Errington, W.J., Herrmann, R., Bönnemann, C., Brockmann, K., Hinderlich, S.,

Lindner, T.H., Steinbrecher, A., et al. (2010). Kelch-like homologue 9 mutation is associated with an early onset autosomal dominant distal myopathy. Brain *133*, 2123–2135.

33. Furukawa, M., He, Y.J., Borchers, C., and Xiong, Y. (2003). Targeting of protein ubiquitination by BTB-Cullin 3-Roc1 ubiquitin ligases. Nat. Cell Biol. *5*, 1001–1007.
34. Canning, P., Cooper, C.D., Krojer, T., Murray, J.W., Pike, A.C., Chaikuad, A., Keates, T., Thangaratnarajah, C., Hojzan, V., Marsden, B.D., et al. (2013). Structural basis for Cul3 protein assembly with the BTB-Kelch family of E3 ubiquitin ligases. J. Biol. Chem. *288*, 7803–7814.
35. Mrosek, M., Labeit, D., Witt, S., Heerklotz, H., von Castelmur, E., Labeit, S., and Mayans, O. (2007). Molecular determinants for the recruitment of the ubiquitin-ligase MuRF-1 onto M-line titin. FASEB J. *21*, 1383–1392.
36. Ravenscroft, G., Sollis, E., Charles, A.K., North, K.N., Baynam, G., and Laing, N.G. (2011). Fetal akinesia: review of the genetics of the neuromuscular causes. J. Med. Genet. *48*, 793–801.
37. Quinn, C.M., Wigglesworth, J.S., and Heckmatt, J. (1991). Lethal arthrogryposis multiplex congenita: a pathological study of 21 cases. Histopathology *19*, 155–162.

Mutations in *B3GALT6*, which Encodes a Glycosaminoglycan Linker Region Enzyme, Cause a Spectrum of Skeletal and Connective Tissue Disorders

Masahiro Nakajima,[1,21] Shuji Mizumoto,[2,21] Noriko Miyake,[3,21] Ryo Kogawa,[2] Aritoshi Iida,[1] Hironori Ito,[4] Hiroshi Kitoh,[5] Aya Hirayama,[6] Hiroshi Mitsubuchi,[7] Osamu Miyazaki,[8] Rika Kosaki,[9] Reiko Horikawa,[10] Angeline Lai,[11] Roberto Mendoza-Londono,[12] Lucie Dupuis,[12] David Chitayat,[12] Andrew Howard,[13] Gabriela F. Leal,[14] Denise Cavalcanti,[15] Yoshinori Tsurusaki,[3] Hirotomo Saitsu,[3] Shigehiko Watanabe,[16] Ekkehart Lausch,[17] Sheila Unger,[18] Luisa Bonafé,[19] Hirofumi Ohashi,[16] Andrea Superti-Furga,[19] Naomichi Matsumoto,[3] Kazuyuki Sugahara,[2] Gen Nishimura,[20] and Shiro Ikegawa[1,*]

Proteoglycans (PGs) are a major component of the extracellular matrix in many tissues and function as structural and regulatory molecules. PGs are composed of core proteins and glycosaminoglycan (GAG) side chains. The biosynthesis of GAGs starts with the linker region that consists of four sugar residues and is followed by repeating disaccharide units. By exome sequencing, we found that *B3GALT6* encoding an enzyme involved in the biosynthesis of the GAG linker region is responsible for a severe skeletal dysplasia, spondyloepimetaphyseal dysplasia with joint laxity type 1 (SEMD-JL1). *B3GALT6* loss-of-function mutations were found in individuals with SEMD-JL1 from seven families. In a subsequent candidate gene study based on the phenotypic similarity, we found that *B3GALT6* is also responsible for a connective tissue disease, Ehlers-Danlos syndrome (progeroid form). Recessive loss-of-function mutations in *B3GALT6* result in a spectrum of disorders affecting a broad range of skeletal and connective tissues characterized by lax skin, muscle hypotonia, joint dislocation, and spinal deformity. The pleiotropic phenotypes of the disorders indicate that *B3GALT6* plays a critical role in a wide range of biological processes in various tissues, including skin, bone, cartilage, tendon, and ligament.

Skeletal dysplasias represent a vast collection of genetic disorders of the skeleton, currently divided into 40 groups.[1] Spondyloepimetaphyseal dysplasia (SEMD) is one group (group 13) of skeletal dysplasia that contains more than a dozen distinctive diseases. SEMD with joint laxity (SEMD-JL) is a subgroup of SEMD that consists of type 1 (SEMD-JL1 [MIM 271640]) and type 2 (SEMD-JL2 [MIM 603546]). SEMD-JL1 or SEMD-JL Beighton type is an autosomal-recessive disorder that shows mild craniofacial dysmorphism (prominent eye, blue sclera, long upper lip, small mandible with cleft palate) and spatulate finger with short nail.[2] The large joints of individuals with SEMD-JL1 are variably affected with hip dislocation, elbow contracture secondary to radial head dislocation, and clubfeet. Joint laxity is particularly prominent in the hands. Skeletal changes of SEMD-JL1 are characterized by moderate platyspondyly with anterior projection of the vertebral bodies, hypoplastic ilia, and mild metaphyseal flaring.[3] Kyphoscoliosis progresses with age, leading to a short trunk, whereas platyspondyly become less conspicuous and the vertebral bodies appear squared in shape with age. Recently, dominant kinesin family member 22 (*KIF22* [MIM 603213]) mutations have been found in SEMD-JL2;[4,5] however, the genetic basis of SEMD-JL1 remains unknown.

To identify the SEMD-JL1-causing mutation, we performed whole-exome sequencing experiments. We recruited seven individuals with SEMD-JL1 from five unrelated Japanese families (F1–F5) and a Singapore/Japanese family (F6) (Table 1). One family (F1) had a pair of affected sibs (P1 and P2) from nonconsanguineous parents. Genomic DNA was extracted by standard procedures

[1]Laboratory for Bone and Joint Diseases, Center for Integrative Medical Sciences, RIKEN, Tokyo 108-8639, Japan; [2]Laboratory of Proteoglycan Signaling and Therapeutics, Frontier Research Center for Post-Genomic Science and Technology, Graduate School of Life Science, Hokkaido University, Sapporo 001-0021, Japan; [3]Department of Human Genetics, Yokohama City University Graduate School of Medicine, Yokohama 236-0004, Japan; [4]Department of Orthopaedic Surgery, Central Hospital, Aichi Prefectural Colony, Kasugai 480-0392, Japan; [5]Department of Orthopaedic Surgery, Nagoya University School of Medicine, Nagoya 466-8550, Japan; [6]Department of Pediatrics, Akita Prefectural Center on Development and Disability, Akita 010-1407, Japan; [7]Department of Neonatology, Kumamoto University Hospital, Kumamoto 860-8556, Japan; [8]Department of Radiology, National Center for Child Health and Development, Tokyo 157-8535, Japan; [9]Division of Medical Genetics, National Center for Child Health and Development, Tokyo 157-8535, Japan; [10]Division of Endocrinology and Metabolism, National Center for Child Health and Development, Tokyo 157-8535, Japan; [11]Department of Paediatric Medicine, KK Women's and Children's Hospital, Singapore 229899, Singapore; [12]Department of Paediatrics, The Hospital for Sick Children and University of Toronto, Toronto, ON M5G 1X8, Canada; [13]Department of Surgery, The Hospital for Sick Children and University of Toronto, Toronto, ON M5G 1X8, Canada; [14]The Professor Fernando Figueira Integral Medicine Institute (IMIP), Recife, PE 50070-550, Brazil; [15]Skeletal Dysplasia Group, Department of Medical Genetics, Faculty of Medical Sciences, State University of Campinas (UNICAMP), Campinas, SP 13083-970, Brazil; [16]Division of Medical Genetics, Saitama Children's Medical Center, Saitama 339-8551, Japan; [17]Division of Paediatric Genetics, Centre for Pediatrics and Adolescent Medicine, University of Freiburg, Freiburg 79106, Germany; [18]Medical Genetics Service, University of Lausanne, CHUV, Lausanne 1011, Switzerland; [19]Department of Pediatrics, University of Lausanne, CHUV, Lausanne 1011, Switzerland; [20]Department of Pediatric Imaging, Tokyo Metropolitan Children's Medical Center, Fuchu 183-8561, Japan
[21]These authors contributed equally to this work
*Correspondence: sikegawa@ims.u-tokyo.ac.jp
http://dx.doi.org/10.1016/j.ajhg.2013.04.003.

Table 1. Clinical and Radiographic Findings of the Individuals with *B3GALT6* Mutations

Subject ID	P1	P2	P3	P4	P5	P6	P7	P8	P9	P10	P11	P12
Family ID	F1	F1	F2	F3	F4	F5	F6	F7	F8	F9	F9	F10
Clinical diagnosis	SEMD-JL1	SEMD-JL1	SEMD-JL1	SEMD-JL1	SEMD-JL1	SEMD-JL1	SEMD-JL1	SEMD-JL1	EDS-PF	EDS-PF	EDS-PF	EDS-PF
General Information												
Ethnicity	Japanese	Japanese	Japanese	Japanese	Japanese	Japanese	Japanese/ Singaporean	Vietnamese	Italian	Italian/ Canadian	Italian/ Canadian	Brazilian
Gender	M	M	F	M	F	F	M	M	M	F	F	F
Age	34 years	31 years	12 years, 7 months	6 years	5 years, 1 month	12 years	2 years, 9 months	34 years	8 months	7 years	1 month	5 years, 1 month
Gestational age	39 weeks, 2 days	full term	37 weeks	40 weeks, 1 day	39 weeks, 5 days	full term	39 weeks	full term	ND	36 weeks	37 weeks	39 weeks
Birth length (cm)	ND	ND	36	ND	43.1	42	43	(average)	ND	44	44	44
Birth weight (g)	ND	2,200	2,124	2,832	2,535	2,222	2,485	3,500	ND	2,097	2,790	3,300
Clinical Features												
Height (cm) (SD)[a]	127.7 (−7.4)	130 (−7.0)	88.8 (−10.7)	94 (−4.0)	90 (−4.0)	118.4 (−5.1)	78.2 (−4.0)	118 (−9.1)	66 (−1.6)	90 (−6.8)	45 (−3.7)	81 (−5.9)
Weight (kg) (SD)[a]	40.3 (−2.2)	36.9 (−2.5)	13.2 (−3.7)	15.4 (−1.5)	14.4 (−1.3)	23.2 (−2.0)	10.6 (−1.9)	28 (−3.3)	5.65 (−3.0)	13.9 (−2.2)	2.65 (−2.8)	8.5 (−8.4)
Craniofacial												
Flat face with prominent forehead	ND	ND	+	+	+	+	+	−	+	+	+	+
Prominent eyes, proptosis	ND	ND	+	−	−	+	+	−	+	+	+	+
Blue sclerae	ND	ND	+	+	+	−	+	−	+	+	+	−
Long upper lip	ND	ND	−	+	+	−	+	+	+	+	+	−
Micrognathia	ND	ND	+	+	+	+	−	+	−	−	−	−
Cleft palate	ND	ND	−	−	−	−	−	−	−	−	−	+
Musculoskeletal												
Kyphoscoliosis[b]	+ (7 months)	+ (1.2 years)	+ (8 months)	+ (infancy)	+ (2 years)	+ (3 months)	+ (8 months)	+ (1 year)	+ (6 months)	++ (prenatal)	++ (prenatal)	++ (2 years)
Spatulate finger	−	ND	+	+	+	+	−	−	+	+	+	−
Finger laxity	ND	ND	+	+	−	−	+	−	++	+	+	+
Large joint laxity	ND	ND	+	+	−	−	+	−	++	++	++	+
Restricted elbow movement	+	ND	+	+	+	−	−	+	+	+	+	+
Hand contracture	−	−	−	−	−	+	−	−	−	+	+	−

(*Continued on next page*)

Table 1. *Continued*

Subject ID	P1	P2	P3	P4	P5	P6	P7	P8	P9	P10	P11	P12
Hip dislocation	–	–	–	+	–	+	–	–	–	+	+	+
Clubfeet	–	–	+	–	–	–	+	–	–	+	+	–
Muscular hypotonia	–	–	+	–	–	–	–	–	++	++	++	++
Skin and Hair												
Doughy skin	ND	ND	+	–	–	–	+	–	++	+	+	+
Hyperextensibility	ND	ND	+	–	–	–	+	–	++	+	+	–
Cutis laxa	ND	ND	–	–	–	–	–	–	+	+	–	+
Sparse hair	ND	ND	–	–	–	–	–	–	+	+	+	–
Others			MR, DD				camptodactyly			DD		pectus excavatum
Radiological Features												
Platyspondyly	+[c]	+[c]	+[c]	+	+	+	+	+	+	+	+	+
Anterior beak of vertebral body[b]	+	+	– (4 years)	– (5 years)	+	+	+	–	+	+	+	+
Short ilia	+	+	+	+	+	+	+	+	+	+	+	+
Prominent lesser trochanter	+	+	+	–	+	+	+	+	+	+	+	+
Metaphyseal flaring	+	+	+	+	+	+	+	+	+	–	+	+
Epiphyseal dysplasia of femoral head	–	–	–	+	–	+	–	–	–	–	+	+
Elbow malalignment	ND	ND	+	+	+	+	+	+	+	+	+	+
Advanced carpal ossification[b]	– (9 years)	ND	– (12 years)	+	+	+	+	ND	+	– (7 years)	–	– (5 years)
Carpal fusion	ND	ND	+	–	–	–	–	–	–	–	–	–
Metacarpal shortening	ND	ND	+	+	+	+	+	+	–	–	+	–
Overtubulation	–	–	–	–	–	–	–	–	+	+	+	+

Abbreviations are as follows: SEMD-JL1, spondyloepimetaphyseal dysplasia with joint laxity type 1; EDS-PF, Ehlers-Danlos syndrome, progeroid form; ND, no data; MR, mitral regurgitation; DD, developmental delay.
[a]At last presentation.
[b]Age at medical attention provided in parentheses.
[c]Absent at age 20 years in P1 and P2 and at age 12 years in P3.

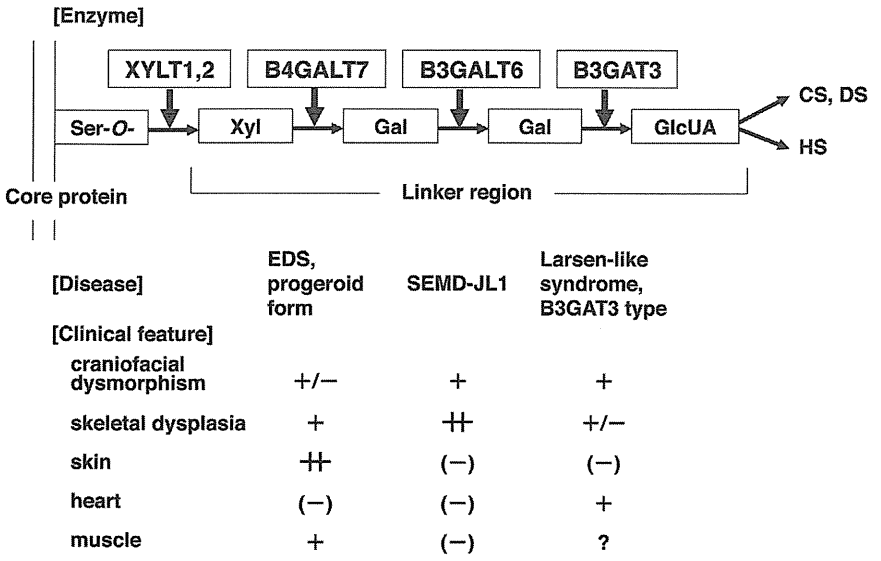

Figure 1. Enzymes Involved in Biosynthesis of the Glycosaminoglycan Linker Region and Summary Features of Diseases Caused by Their Defects Based on a Conventional Concept for the Diseases

The biosyntheses of GAGs start with the formation of a common tetrasaccharide linker sequence covalently attached to the core protein. The linker region synthesis involves a single linear pathway composed of four successive steps catalyzed by distinctive enzymes. Abbreviations are as follows: XYLT, β-xylosyltransferase; B4GALT7, xylosylprotein β1,4-galactosyltransferase, polypeptide 7 (β1,4-galactosyltransferase-I); B3GALT6, UDP-Gal, βGal β1,3-galactosyltransferase polypeptide 6 (β1,3-galactosyltransferase-II); B3GAT3, β-1,3-glucuronyltransferase 3 (glucuronosyltransferase I); Ser-*O*, the serine residue of the GAG attachment site on the proteoglycan core protein; Xyl, xylose; Gal, galactose; GlcUA, D-glucuronic acid; CS, chondroitin sulfate; DS, dermatan sulfate; HS, heparan sulfate; EDS, Ehlers-Danlos syndrome; SEMD-JL1, spondyloepimetaphyseal dysplasia with joint laxity type 1.

from peripheral blood, saliva, or Epstein-Barr virus-immortalized lymphocyte of the individuals with SEMD-JL1 and/or their parents after informed consent. The study was approved by the ethical committee of RIKEN and participating institutions. We captured the exomes of the seven subjects as previously described.[6,7] In brief, we sheared genomic DNA (3 μg) by Covaris S2 system (Covaris) and processed with a SureSelect All Exon V4 kit (Agilent Technologies). We sequenced DNAs captured by the kit with HiSeq 2000 (Illumina) with 101 base pair-end reads. We performed the image analysis and base calling by HiSeq Control Software/Real Time Analysis and CASAVA1.8.2 (Illumina) and mapped the sequences to human genome hg19 by Novoalign. We processed the aligned reads by Picard to remove PCR duplicate. The mean depth of coverage for reads was 132.8×, and, on average, 91.0% of targeted bases had sufficient coverage (20× coverage) and quality for variant calling (Table S1 available online). The variants were called by Genome Analysis Toolkit 1.5-21 (GATK) with the best practice variant detection with the GAKT v.3 and annotated by ANNOVAR (2012 February 23).

Based on the hypothesis that SEMD-JL1 is inherited in an autosomal-recessive fashion, we filtered variants with the script created by BITS (Tokyo, Japan) according to following conditions: (1) variants registered in ESP5400, (2) variants found in our in-house controls (n = 274), (3) synonymous changes, (4) rare variants registered in dbSNP build 135 (MAF < 0.01), and (5) variants associated with segmental duplication. After combining variants selected by the homozygous mutation model and the compound heterozygous mutation model, we selected genes shared by individuals from three or more families. The analysis of the next-generation sequencing identified possible compound heterozygous variants in *B3GALT6* in individuals from three families (Table S2). In addition, two other subjects had possible causal heterozygous variants of *B3GALT6*.

B3GALT6 (RefSeq accession number NM_080605.3) is a single-exon gene on chromosome 1p36.33. It encodes UDP-Gal:βGal β1,3-galactosyltransferase polypeptide 6 (or galactosyltransferase-II: GalT-II), an enzyme involved in the biosynthesis of the glycosaminoglycan (GAG) linker region.[8] The biosyntheses of dermatan sulfate (DS), chondroitin sulfate (CS), and heparin/heparan sulfate (HS) GAGs start with the formation of a tetrasaccharide linker sequence, glucuronic acid-β1-3-galactose-β1-3-galactose-β1-4-xylose-β1 (GlcUA-Gal-Gal-Xyl), which is covalently attached to the core protein. The linker region synthesis involves a single linear pathway composed of four successive steps catalyzed by distinctive enzymes (Figure 1). The first step is the addition of xylose to the hydroxy group of specific serine residues on the core protein by xylosyltransferases from UDP-Xyl, followed by two distinct galactosyltransferases (GalT-I and II) and a glucuronosyltransferase from UDP-Gal and UDP-GlcUA, respectively. The next hexosamine addition is critical because it determines which GAG (i.e., CS, DS, or HS) is assembled on the linker region. GalT-II encoded by *B3GALT6* functions in the third step of the linker formation (Figure 1).

To confirm the results obtained by the next-generation sequencing, we examined the seven subjects used for the next-generation sequencing and an additional subject from a Vietnamese family (F7) by direct sequence of the PCR products from genomic DNAs using 3730xl DNA Analyzer (Applied Biosystems). The Sanger sequencing confirmed all *B3GALT6* mutations found by the next-generation sequencing and identified additional *B3GALT6* mutations. The results indicated that *B3GALT6* mutations were found in all subjects (Tables 2 and S1). All but P4 from F3 were compound heterozygotes of missense mutations. In P4, only a heterozygous c.1A>G (p.Met1?) mutation was found, although we searched for a *B3GALT6* mutation in the entire coding region, 5′ and 3′ UTRs, and flanking

Table 2. *B3GALT6* Mutations in Spondyloepimetaphyseal Dysplasia with Joint Laxity Type 1 and Ehlers-Danlos Syndrome, Progeroid Form

Family	Clinical Diagnosis	Nucleotide Change	Amino Acid Change
F1	SEMD-JL1	c.1A>G	p.Met1?
		c.694C>T	p.Arg232Cys
F2	SEMD-JL1	c.1A>G	p.Met1?
		c.466G>A	p.Asp156Asn
F3[a]	SEMD-JL1	c.1A>G	p.Met1?
F4	SEMD-JL1	c.1A>G	p.Met1?
		c.694C>T	p.Arg232Cys
F5	SEMD-JL1	c.694C>T	p.Arg232Cys
		c.899G>C	p.Cys300Ser
F6	SEMD-JL1	c.1A>G	p.Met1?
		c.193A>G	p.Ser65Gly
F7	SEMD-JL1	c.200C>T	p.Pro67Leu
		c.694C>T	p.Arg232Cys
F8	EDS-PF	c.353delA	p.Asp118Alafs*160
		c.925T>A	p.Ser309Thr
F9	EDS-PF	c.588delG	p.Arg197Alafs*81
		c.925T>A	p.Ser309Thr
F10	EDS-PF	c.16C>T	p.Arg6Trp
		c.415_423del	p.Met139Ala141del

The nucleotide changes are shown with respect to *B3GALT6* mRNA sequence. The corresponding predicted amino acid changes are numbered from the initiating methionine residue.
[a]Only a heterozygous mutation was found.

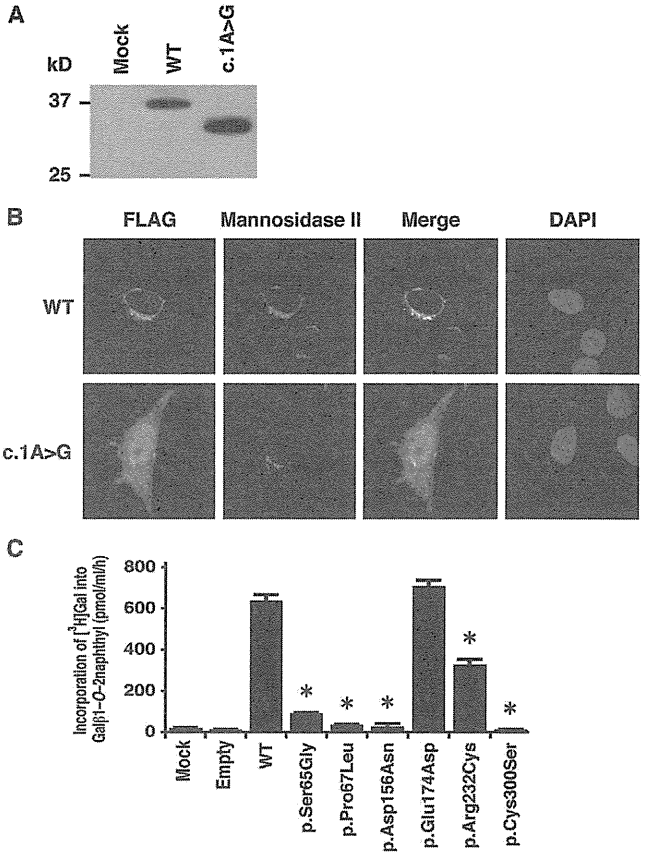

Figure 2. Analyses of B3GALT6 Missense Mutant Proteins Identified in Individuals with SEMD-JL1 In Vitro
(A) Immunoblot analysis of lysates from HeLa cells expressing transfected wild-type (WT) and mutant (c.1A>G) *B3GALT6*. The mutant *B3GALT6* yields a shortened protein. The difference of the molecular sizes between WT and mutant proteins is approximately ~4 kD.
(B) Subcellular localization of B3GALT6. HeLa cells were transfected with WT and mutant (c.1A>G) *B3GALT6*. Cells were stained with anti-FLAG (green), anti-α-mannosidase II (red), and 4′,6-diamidino-2-phenylindole (DAPI; blue). WT was expressed in the Golgi, but the mutant was found in cytoplasm and nucleus.
(C) Decreased enzyme activities of the missense mutant proteins (p.Ser65Gly, p.Pro67Lys, p.Asp156Asn, p.Arg232Cys, and p.Cys300Ser). p.Glu174Asp is a common polymorphism in the public database. The GalT-II activity is measured by incorporation of [^{3}H]Gal into Galβ1-*O*-2naphthyl (*p*mol/ml/hr) and represents the averages of three independent experiments performed in triplicate. Empty and mock indicate the GalT-II activity obtained with the conditioned medium transfected with or without an empty vector. *$p < 0.0001$ versus WT (one-way analysis of variance with Dunnett's adjustment).

regions of *B3GALT6*. Most of the mutations are predicted to be disease causing by in silico analysis. The c.1A>G (p.Met1?) mutation was found in individuals from five of the seven families.

Although mutations affecting initiation codons have been reported to be pathogenic in several diseases,[9] the effects of initiation codon mutations on the encoded protein are variable among the genes. We therefore investigated the effect of the c.1A>G (p.Met1?) mutation on the protein by using C-terminally FLAG-tagged B3GALT6 with and without the mutation expressed in HeLa cells (RIKEN Cell Bank). We detected the mutant B3GALT6 protein with a molecular weight ~4 kD lower compared with the wild-type (WT) protein (Figure 2A). These results suggest that translation initiation at the second ATG of the coding sequence, at position c.124, would become the initiation codon because of the mutation, probably resulting in an N-terminal deletion of 41 amino acids (p.Met1_Ala41del), in the same open reading frame that contains the transmembrane domain. We then examined the subcellular localization of the mutant B3GALT6 protein by immunocytochemistry. The immunofluorescence for WT-B3GALT6 was observed in a perinuclear region overlapping with that for α-mannosidase II, a marker of the Golgi as previously reported.[8] In contrast, the immunofluorescence for the mutant B3GALT6 protein was observed in the nucleus and cytoplasm (Figure 2B). Therefore, the mutant protein can be considered to be functionally null because of the mislocalization.

To investigate the causality of other *B3GALT6* missense mutations, we also examined the subcellular localization of the mutant B3GALT6 proteins by immunocytochemistry. c.193A>G (p.Ser65Gly), c.200C>T (p.Pro67Leu),

and c.694C>T (p.Arg232Cys) mutants showed mislocalization, whereas c.466G>A (p.Asp156Asn) and c.899G>C (p.Cys300Ser) mutants showed normal localization (Figure S1). To investigate whether the *B3GALT6* missense mutations affect the enzyme function, the GalT-II activities of soluble FLAG-tagged proteins for WT and mutant B3GALT6 proteins were assayed. The GalT-II activities of p.Ser65Gly-, p.Pro67Leu-, p.Asp156Asn-, p.Arg232Cys-, and p.Cys300Ser-B3GALT6 were significantly decreased compared with WT-B3GALT6 (Figure 2C), indicating that these mutations resulted in a loss of enzyme function. On the other hand, there were no significant differences in the GalT-II activities between WT-B3GALT6 and p.Glu174Asp-B3GALT6, a common polymorphism (rs12085009) in the public database (Figure 2C).

All SEMD-JL1 individuals with the *B3GALT6* mutation had the characteristic skeletal abnormalities, including platyspondyly, short ilia, and elbow malalignment (Table 1 and Figure S2); however, some had a range of extraskeletal and connective tissue abnormalities that overlapped with those seen in Ehlers-Danlos syndrome, progeroid form (EDS-PF [MIM 130070]). EDS-PF is an autosomal-recessive connective tissue disorder characterized by sparse hair, wrinkled skin, and defective wound healing with atrophic scars.[10] In addition, skeletal abnormalities so far reported in EDS-PF are limited to generalized osteopenia and radial head dislocation, which are in contrast with the severe generalized dysplasias of the axial and appendicular skeleton observed in SEMD-JL1. Thus, both disorders at first glance appear as separate clinical entities, although they share the clinical features of short stature, joint laxity and dislocation, and facial dysmorphism. In two families with individuals with EDS-PF, recessive mutations of *B4GALT7* (MIM 604327) have been found.[11,12] *B4GALT7* (RefSeq NM_007255.2) encodes an enzyme, xylosylated protein β-1,4-galactosyltransferase, that catalyzes the second step of the GAG linker region biosynthesis (Figure 1). Therefore, we speculated that B3GALT6 and B4GALT7 deficiencies might show similar phenotypes. We then examined *B3GALT6* in four additional individuals (P9–P12) who had phenotypes compatible with EDS-PF (Table 1 and Figure S3) but in whom no *B4GALT7* mutations had been found. Sanger sequencing of the EDS-PF-like subjects revealed that all were compound heterozygotes for *B3GALT6* mutations (Table 2). There were two frameshift mutations and one missense mutation (c.925T>A [p.Ser309Thr]) common in two families (F8 and F9). We investigated the enzyme function of the missense mutation by using the same assay for SEMD-JL1 missense mutations. The GalT-II activities of p.Ser309Thr-B3GALT6 were significantly decreased (Figure S4).

Collectively, 11 different mutations in individuals from 10 families were identified in *B3GALT6* by a combination of exome and targeted sequencing (Table 2 and Figure S5). None of these mutations were detected in more than 200 ethnicity-matched controls or in public databases, including the 1000 Genomes database, indicating that they are unlikely to be polymorphisms. SEMD-JL1 and EDS-PF-like individuals had no common mutations (Table 2). The individuals with *B3GALT6* mutations were short at birth and their short stature worsened with age. Their common clinical features were a flat face with prominent forehead and kyphoscoliosis (Table 1). Kyphoscoliosis was noticed in infancy in most cases and even in utero in severe cases. Although skeletal changes were essentially the same, craniofacial and skin abnormalities, joint laxities, and muscular hypotonia were variable among the individuals with *B3GALT6* mutations. Common radiographic features were platyspondyly that becomes less conspicuous with age, short ilia, and elbow malalignment (Table 1). Prominent lesser trochanters and metaphyseal flaring were seen in most cases. No individuals showed generalized osteoporosis. The disease phenotype was very variable between families (mutations), but in two familial cases, phenotypes were similar between the pair of the sibs. As a corollary, our results indicate that EDS-PF is genetically heterogeneous, with a proportion of cases being caused by mutations in *B4GALT7* and another in *B3GALT6*.

Diseases caused by defects in enzymes involved in the biosynthesis of the GAG linker region are categorized as the GAG linkeropathy. The first member of GAG linkeropathy has been identified to arise from an EDS-PF/B4GALT7 deficiency. *B4GALT7* mutations have been identified in homozygous c.808C>T (p.Arg270Cys)[12] and compound heterozygous (c.557C>A [p.Ala186Asp] and c.617T>C [p.Leu206Pro])[11] states. Another member of GAG linkeropathy manifests itself as Larsen-like syndrome, B3GAT3 type (MIM 245600). A family with individuals harboring a homozygous *B3GAT3* (MIM 606374; RefSeq NM_012200.3) mutation (c.830G>A [p.Arg227Gln]) has been identified. The clinical features of five affected individuals of the family are characterized by dislocation and laxity of joints and congenital heart defects.[11] The former considerably overlaps with the phenotypes of SEMD-JL1 and EDS-PF, two other GAG linkeropathies; however, the association of heart defects has critically differentiated this disease from the others (Figure 1).

Given that the linker region biosynthesis is nonparallel and that the defects in the three enzymes simply affect the amounts of the linker region available to form GAGs (CS, HS, DS), phenotypic similarities of the three diseases are quite understandable. The quantitative difference of the phenotypes (severity of the diseases) most probably results from the difference in the degree of enzyme defects resulting from mutations. On the other hand, qualitative differences of the three diseases (e.g., scoliosis caused by the *B3GALT6* mutation, heart disease caused by the *B3GAT3* mutation, etc.) suggest other explanations. Tissue expression patterns of the three genes do not entirely explain the differences. We examined their mRNA expression in various human tissues, including cartilage, bone, and connective tissues by quantitative real-time PCR (Figure S6). We detected strong expression of *B3GALT6* in

Table 3. The Amount of GAGs in the Lymphoblastoid Cells from Individuals with Spondyloepimetaphyseal Dysplasia with Joint Laxity Type 1

	GAG (Disaccharides/mg Acetone Powder)[a] [pmol]			
Subject	**CS/DS**	**CS**	**DS**	**HS**
Control	62	48	29	128
SEMD-JL1				
P1	313	295	118	15
P2	345	175	60	21
P3	270	162	28	20

[a]Calculated based on the peak area in chromatograms of digests with a mixture of chondroitinases ABC and AC-II (CS/DS), chondroitinases AC-I and AC-II (CS), chondroitinase B (DS), and heparinases I and III (HS).

cartilage and bone but only weak expression in skin, ligament, and tendon. *B4GALT7* expression was stronger in cartilage than *B3GALT6* and also weak in skin and ligament. *B3GAT3* expression was not specific to heart. The qualitative difference may result from the difference in the effects of the three genes on GAG formation.

To examine how *B3GALT6* mutations affects the products of GAGs in vivo, we measured the amounts of CS and HS chains at the surface of lymphoblastoid cells from the subjects by flow cytometry by using CS-stub and HS-stub antibodies as previously described.[13–15] In brief, purified GAG fractions were treated individually with a mixture of chondroitinases ABC and AC-II, a mixture of chondroitinases AC-I (EC 4.2.2.5) (Seikagaku Corp.) and AC-II (EC 4.2.2.5) (Seikagaku Corp.), chondroitinase B (EC 4.2.2.19) (IBEX Technologies), or a mixture of heparinases-I and -III (IBEX Technologies) for analyzing the disaccharide composition of CS/DS, CS, DS, and HS, respectively. The digests were labeled with a fluorophore 2-aminobenzamide (2AB) and aliquots of the 2AB derivatives of CS/DS/HS disaccharides were analyzed by anion-exchange HPLC on a PA-03 column (YMC Co.). The HS-stub antibody (3G10) showed a markedly reduced binding to the epitopes on the subjects' cells (Figure S7). The relative numbers of the HS chains presented as the mean fluorescence intensity (MFI) of the cell population stained with the antibody for P1, P2, and P3 were 26%, 56%, and 35% of the control, respectively. On the other hand, the CS-stub antibody (2B6) showed a similar binding to the epitopes on the subjects' cells relative to those of the control (Figure S7). The MFI for P1, P2, and P3 were 114%, 104%, and 106% of the control, respectively. Furthermore, we measured disaccharide of GAG chains from lymphoblastoid cells by using anion-exchange HPLC after digestion with chondroitinase and heparinase. The amounts of the disaccharide from HS chains were significantly decreased, whereas CS and DS chains were ~5 times higher than those in the control (Table 3).

Previous biochemical studies on EDS-PF with *B4GALT7* mutations show a reduction in the synthesis of DS chains.[16,17] The c.830G>A (p.Arg227Gln) mutation in *B3GAT3* causes a drastic reduction in GlcAT-I activity in fibroblasts of the individual with SEMD-JL1 and numbers of CS and HS chains on the core proteins at the surface of the fibroblasts are decreased to about half of the controls.[11] Cultured lymphoblastoid cells from individuals with a c.419C>T (p.Pro140Leu) mutation in *B3GAT3* show that defective synthesis is more pronounced for CS than for HS.[11] Taken together with our results, these findings suggest that the effects of the deficiencies of the three enzymes on GAG synthesis are not identical. A possible explanation for the qualitative phenotypic differences may be that the biosynthesis of the GAG linker region is not a simple step-by-step addition but involves parallel processing and/or alternative pathways. Other glycosyltransferases may have similar biochemical functions to these three enzymes and thus complement their deficient activities to variable degrees in cell- and/or tissue-specific manners, leading to differences in the amount of GAGs in the tissues. It is known that B3GALT6 and B4GALT7 have several homologs.[18] It must be noted that all biochemical studies so far have been performed in vitro or in cultured cells, and therefore there is a severe limitation to our understanding of the pathogenesis at tissue and organ levels.

By exome sequencing, we identified loss-of-function mutations in *B3GALT6* in 12 individuals from 10 families. The mutations produced a spectrum of connective tissue disorders characterized by lax skin, muscle hypotonia, joint dislocation, and skeletal dysplasia and deformity, which include phenotypes previously known as SEMD-JL1 and EDS-PF (Figures S1 and S2). The pleiotropic phenotypes of *B3GALT6* mutations indicate that B3GALT6 plays critical roles in development and homeostasis of various tissues, including skin, bone, cartilage, tendons, and ligaments. Biochemical studies that used lymphoblastoid cells of the individuals with *B3GALT6* mutations showed a decrease of HS and a paradoxical increase of CS and DS of the cell surface. Further clinical, genetic, and biological studies are necessary to understand the pathological mechanism of the diseases caused by enzyme defects involved in the biosynthesis of the GAG linker region and roles of the region in GAG metabolism and function.

Supplemental Data

Supplemental Data include seven figures and two tables and can be found with this article online at http://www.cell.com/AJHG/.

Acknowledgments

We thank the individuals with the disease and their family for their help to the study. We also thank the Japanese Skeletal Dysplasia Consortium. This study is supported by research grants from the Ministry of Health, Labor, and Welfare (23300101 to S.I. and N. Matsumoto; 23300201 to S.I.), by Grants-in-Aid for Young Scientists (23689052 to N. Miyake and 23790066 to S.M.) from the Japan Society for the Promotion of Science; by the Matching Program for Innovations in Future Drug Discovery and Medical Care

(K.S.); by The Ministry of Education, Culture, Sports, Science and Technology, Japan (MEXT); by a Grant-in-aid for Encouragement from the Akiyama Life Science Foundation (S.M.); by Swiss National Science Foundation Grants (31003A_141241 and 310030_132940); by The CoSMO-B project (Brazil and Switzerland); by the Leenaards Foundation (Switzerland); and by Research on intractable diseases, Health and Labour Sciences Research Grants, H23-Nanchi-Ippan-123 (S.I.).

Received: February 1, 2013
Revised: March 16, 2013
Accepted: April 5, 2013
Published: May 9, 2013

Web Resources

The URLs for data presented herein are as follows:

1000 Genomes, http://browser.1000genomes.org
ANNOVAR, http://www.openbioinformatics.org/annovar/
dbSNP, http://www.ncbi.nlm.nih.gov/projects/SNP/
GATK, http://www.broadinstitute.org/gatk/
MutationTaster, http://www.mutationtaster.org/
NHLBI Exome Sequencing Project (ESP) Exome Variant Server, http://evs.gs.washington.edu/EVS/
Novoalign, http://www.novocraft.com/main/page.php?s=novoalign
Online Mendelian Inheritance in Man (OMIM), http://www.omim.org/
Picard, http://picard.sourceforge.net/
PolyPhen, http://www.genetics.bwh.harvard.edu/pph2/
RefSeq, http://www.ncbi.nlm.nih.gov/RefSeq
SIFT, http://sift.bii.a-star.edu.sg/
UCSC Genome Browser, http://genome.ucsc.edu

References

1. Warman, M.L., Cormier-Daire, V., Hall, C., Krakow, D., Lachman, R., LeMerrer, M., Mortier, G., Mundlos, S., Nishimura, G., Rimoin, D.L., et al. (2011). Nosology and classification of genetic skeletal disorders: 2010 revision. Am. J. Med. Genet. A. *155A*, 943–968.
2. Beighton, P., Gericke, G., Kozlowski, K., and Grobler, L. (1984). The manifestations and natural history of spondylo-epi-metaphyseal dysplasia with joint laxity. Clin. Genet. *26*, 308–317.
3. Nishimura, G., Satoh, M., Aihara, T., Aida, N., Yamamoto, T., and Ozono, K. (1998). A distinct subtype of "metatropic dysplasia variant" characterised by advanced carpal skeletal age and subluxation of the radial heads. Pediatr. Radiol. *28*, 120–125.
4. Boyden, E.D., Campos-Xavier, A.B., Kalamajski, S., Cameron, T.L., Suarez, P., Tanackovic, G., Andria, G., Ballhausen, D., Briggs, M.D., Hartley, C., et al. (2011). Recurrent dominant mutations affecting two adjacent residues in the motor domain of the monomeric kinesin KIF22 result in skeletal dysplasia and joint laxity. Am. J. Hum. Genet. *89*, 767–772.
5. Min, B.J., Kim, N., Chung, T., Kim, O.H., Nishimura, G., Chung, C.Y., Song, H.R., Kim, H.W., Lee, H.R., Kim, J., et al. (2011). Whole-exome sequencing identifies mutations of KIF22 in spondyloepimetaphyseal dysplasia with joint laxity, leptodactylic type. Am. J. Hum. Genet. *89*, 760–766.
6. Miyake, N., Elcioglu, N.H., Iida, A., Isguven, P., Dai, J., Murakami, N., Takamura, K., Cho, T.J., Kim, O.H., Hasegawa, T., et al. (2012). PAPSS2 mutations cause autosomal recessive brachyolmia. J. Med. Genet. *49*, 533–538.
7. Tsurusaki, Y., Okamoto, N., Ohashi, H., Kosho, T., Imai, Y., Hibi-Ko, Y., Kaname, T., Naritomi, K., Kawame, H., Wakui, K., et al. (2012). Mutations affecting components of the SWI/SNF complex cause Coffin-Siris syndrome. Nat. Genet. *44*, 376–378.
8. Bai, X., Zhou, D., Brown, J.R., Crawford, B.E., Hennet, T., and Esko, J.D. (2001). Biosynthesis of the linkage region of glycosaminoglycans: cloning and activity of galactosyltransferase II, the sixth member of the beta 1,3-galactosyltransferase family (beta 3GalT6). J. Biol. Chem. *276*, 48189–48195.
9. Saunders, C.J., Minassian, B.E., Chow, E.W., Zhao, W., and Vincent, J.B. (2009). Novel exon 1 mutations in MECP2 implicate isoform MeCP2_e1 in classical Rett syndrome. Am. J. Med. Genet. A. *149A*, 1019–1023.
10. Kresse, H., Rosthøj, S., Quentin, E., Hollmann, J., Glössl, J., Okada, S., and Tønnesen, T. (1987). Glycosaminoglycan-free small proteoglycan core protein is secreted by fibroblasts from a patient with a syndrome resembling progeroid. Am. J. Hum. Genet. *41*, 436–453.
11. Baasanjav, S., Al-Gazali, L., Hashiguchi, T., Mizumoto, S., Fischer, B., Horn, D., Seelow, D., Ali, B.R., Aziz, S.A., Langer, R., et al. (2011). Faulty initiation of proteoglycan synthesis causes cardiac and joint defects. Am. J. Hum. Genet. *89*, 15–27.
12. Faiyaz-Ul-Haque, M., Zaidi, S.H., Al-Ali, M., Al-Mureikhi, M.S., Kennedy, S., Al-Thani, G., Tsui, L.C., and Teebi, A.S. (2004). A novel missense mutation in the galactosyltransferase-I (B4GALT7) gene in a family exhibiting facioskeletal anomalies and Ehlers-Danlos syndrome resembling the progeroid type. Am. J. Med. Genet. A. *128A*, 39–45.
13. Kinoshita, A., and Sugahara, K. (1999). Microanalysis of glycosaminoglycan-derived oligosaccharides labeled with a fluorophore 2-aminobenzamide by high-performance liquid chromatography: application to disaccharide composition analysis and exosequencing of oligosaccharides. Anal. Biochem. *269*, 367–378.
14. Miyake, N., Kosho, T., Mizumoto, S., Furuichi, T., Hatamochi, A., Nagashima, Y., Arai, E., Takahashi, K., Kawamura, R., Wakui, K., et al. (2010). Loss-of-function mutations of CHST14 in a new type of Ehlers-Danlos syndrome. Hum. Mutat. *31*, 966–974.
15. Mizumoto, S., and Sugahara, K. (2012). Glycosaminoglycan chain analysis and characterization (Glycosylation/Epimerization). In Methods in Molecular Biology. In Proteoglycans: Methods and Protocols, F. Rédini, ed. (New York, USA: Humana Press, Springer), pp. 99–115.
16. Okajima, T., Fukumoto, S., Furukawa, K., and Urano, T. (1999). Molecular basis for the progeroid variant of Ehlers-Danlos syndrome. Identification and characterization of two mutations in galactosyltransferase I gene. J. Biol. Chem. *274*, 28841–28844.
17. Quentin, E., Gladen, A., Rodén, L., and Kresse, H. (1990). A genetic defect in the biosynthesis of dermatan sulfate proteoglycan: galactosyltransferase I deficiency in fibroblasts from a patient with a progeroid syndrome. Proc. Natl. Acad. Sci. USA *87*, 1342–1346.
18. Togayachi, A., Sato, T., and Narimatsu, H. (2006). Comprehensive enzymatic characterization of glycosyltransferases with a beta3GT or beta4GT motif. Methods Enzymol. *416*, 91–102.

nature genetics

De novo mutations in the autophagy gene *WDR45* cause static encephalopathy of childhood with neurodegeneration in adulthood

Hirotomo Saitsu[1,10], Taki Nishimura[2,3,10], Kazuhiro Muramatsu[4,10], Hirofumi Kodera[1], Satoko Kumada[5], Kenji Sugai[6], Emi Kasai-Yoshida[5], Noriko Sawaura[4], Hiroya Nishida[7], Ai Hoshino[7], Fukiko Ryujin[8], Seiichiro Yoshioka[8], Kiyomi Nishiyama[1], Yukiko Kondo[1], Yoshinori Tsurusaki[1], Mitsuko Nakashima[1], Noriko Miyake[1], Hirokazu Arakawa[4], Mitsuhiro Kato[9], Noboru Mizushima[2,3] & Naomichi Matsumoto[1]

Static encephalopathy of childhood with neurodegeneration in adulthood (SENDA) is a recently established subtype of neurodegeneration with brain iron accumulation (NBIA)[1–3]. By exome sequencing, we found *de novo* heterozygous mutations in *WDR45* at Xp11.23 in two individuals with SENDA, and three additional *WDR45* mutations were identified in three other subjects by Sanger sequencing. Using lymphoblastoid cell lines (LCLs) derived from the subjects, aberrant splicing was confirmed in two, and protein expression was observed to be severely impaired in all five. *WDR45* encodes WD-repeat domain 45 (WDR45). WDR45 (also known as WIPI4) is one of the four mammalian homologs of yeast Atg18, which has an important role in autophagy[4,5]. Lower autophagic activity and accumulation of aberrant early autophagic structures were demonstrated in the LCLs of the affected subjects. These findings provide direct evidence that an autophagy defect is indeed associated with a neurodegenerative disorder in humans.

NBIA is a heterogeneous group of neurodegenerative diseases that are characterized by a prominent extrapyramidal movement disorder, intellectual deterioration and deposition of iron in the basal ganglia[1–3]. Mutations in several genes involved in diverse cellular processes cause NBIA[6]. SENDA is a recently established subtype of NBIA. SENDA begins with early childhood psychomotor retardation, which remains static until adulthood. Then, during their twenties to early thirties, affected individuals develop sudden-onset progressive dystonia-parkinsonism and dementia. In addition to iron deposition in the globus pallidus and substantia nigra, individuals with SENDA have a distinct pattern on brain magnetic resonance images (MRI) of T1-weighted signal hyperintensity of the substantia nigra, with a central band of hypointensity[1–3,6,7]. SENDA is always sporadic[6,7], suggesting the involvement of *de novo* mutations or autosomal recessive traits. To identify *de novo* or recessive mutations, family-based exome sequencing was performed including the affected individual, an unaffected sibling and the unaffected parents.

A total of 180 and 187 rare protein-altering and splice-site variants were identified per affected subject, which were absent in dbSNP135 data and in 88 in-house control exomes (**Supplementary Table 1**). All genes in each subject were surveyed for *de novo* mutations and compound heterozygous or homozygous mutations that were consistent with an autosomal recessive trait in each family (**Supplementary Table 2**). Two *de novo* and one autosomal recessive candidate mutations were found in subject 1, and a *de novo* candidate mutation was found in subject 2. Only mutations in *WDR45* at Xp11.23, encoding WDR45 (referred to here as WIPI4), were common in the two subjects. A canonical splice-site mutation (c.439+1G>T) was found in subject 1, and a synonymous mutation located at the last base of exon 8 (c.516G>C) was found in subject 2, both of which occurred *de novo* (**Fig. 1a**). Sanger sequencing of *WDR45* in three other affected subjects identified one nonsense and two frameshift mutations (**Fig. 1a**). The c.1033_1034dupAA mutation in subject 5 occurred *de novo*. Parental samples for the other two subjects were unavailable. None of the five mutations were found in 6,500 National Heart, Lung, and Blood Institute (NHLBI) exomes or among our 212 in-house control exomes. All subjects with a *WDR45* mutation are female.

To examine the effects of the mutations on *WDR45* transcription, RT-PCR and sequencing were performed on total RNA extracted from the LCLs of subjects. The c.439+1G>T mutation in subject 1 and the c.516G>C mutation in subject 2 caused 24-bp in-frame and 22-bp

[1]Department of Human Genetics, Graduate School of Medicine, Yokohama City University, Yokohama, Japan. [2]Department of Physiology and Cell Biology, Graduate School and Faculty of Medicine, Tokyo Medical and Dental University, Tokyo, Japan. [3]Department of Biochemistry and Molecular Biology, Graduate School and Faculty of Medicine, The University of Tokyo, Tokyo, Japan. [4]Department of Pediatrics, Gunma University Graduate School of Medicine, Gunma, Japan. [5]Department of Neuropediatrics, Tokyo Metropolitan Neurological Hospital, Tokyo, Japan. [6]Department of Child Neurology, National Center of Neurology and Psychiatry, Tokyo, Japan. [7]Department of Pediatrics, National Rehabilitation Center for Children with Disabilities, Tokyo, Japan. [8]Department of Pediatrics, Shiga University of Medical Science, Shiga, Japan. [9]Department of Pediatrics, Yamagata University Faculty of Medicine, Yamagata, Japan. [10]These authors contributed equally to this work. Correspondence should be addressed to H.S. (hsaitsu@yokohama-cu.ac.jp), N. Mizushima (nmizu@m.u-tokyo.ac.jp) or N. Matsumoto (naomat@yokohama-cu.ac.jp).

Received 24 October 2012; accepted 29 January 2013; published online 24 February 2013; doi:10.1038/ng.2562

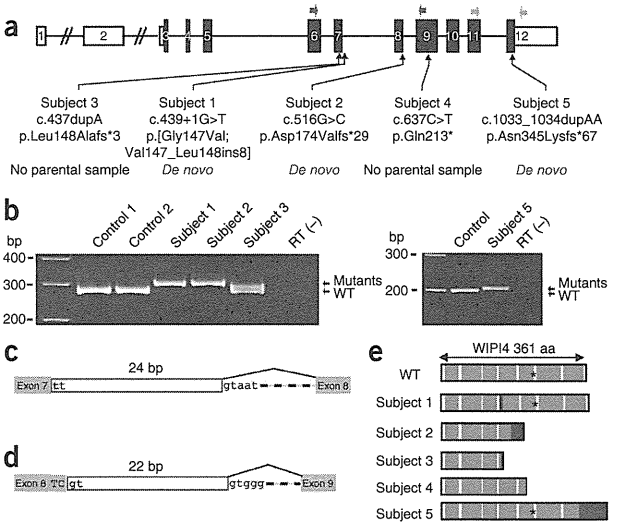

Figure 1 Heterozygous *WDR45* mutations in individuals with SENDA. (**a**) Schematic of *WDR45*, which comprises 12 exons (rectangles). The UTRs and coding region are shown in white and black, respectively. Three mutations were confirmed as *de novo*; the others were unable to be confirmed because parental samples were unavailable. Blue and green arrows indicate the locations of the two sets of primers used in mRNA analysis. (**b**) RT-PCR analysis using the blue primer set (left) and green primer set (right) from **a**. Whereas control cDNA samples showed a single product corresponding to the wild-type allele (WT), an apparently longer product was observed in subjects 1, 2 and 5, indicating that only the transcripts from the mutant allele were expressed. In subject 3, both wild-type and mutant alleles were expressed. Template without reverse transcriptase was used as a negative control, RT(–). (**c**) Schematic of the mutant transcript resulting from the c.439+1G>T mutation (red) in subject 1. A 24-bp insertion caused by the use of a cryptic splice donor site within intron 7 was observed, resulting in a p.Gly147Val substitution followed by an in-frame eight-amino-acid insertion (p.[Gly147Val; Val147_Leu148ins8]). (**d**) Schematic of the mutant transcript resulting from the c.516G>C mutation (red) in subject 2. A 22-bp insertion from the use of a cryptic splice donor site within intron 8 was observed, leading to a frameshift (p.Asp174Valfs*29). (**e**) Schematic of mutant WIPI4 proteins. β-propeller structures and additional residues caused by mutations are colored in blue and red, respectively. The amino-acid residues of the mutant protein predicted from cDNA sequences are shown in relation to seven–β propeller structures[13–15]. An asterisk indicates the position of the FRRG motifs.

frameshift insertions, respectively (**Fig. 1b–d** and **Supplementary Fig. 1**). The c.437dupA, c.637C>T and c.1033_1034dupAA mutations were confirmed in the transcripts (**Fig. 1b** and **Supplementary Fig. 1**). Theoretically, mutant WIPI4 would be severely truncated in subjects 2, 3 and 4 and relatively conserved in subjects 1 and 5 (**Fig. 1e**). As human female cells are subject to X-chromosome inactivation, subjects with a *WDR45* mutation may have two cell populations: one expressing a wild-type allele and the other expressing a mutant allele. Notably, whereas both wild-type and mutant alleles were expressed in the LCLs of subject 3, the LCLs of the other four affected subjects exclusively expressed mutant transcripts, suggesting that the wild-type alleles underwent X inactivation in most cells (**Fig. 1b** and **Supplementary Fig. 1**). In fact, X-inactivation analysis with genomic DNA from peripheral leukocytes showed a skewed pattern in subjects 2, 4 and 5 (analysis was non-informative in subject 1) (**Supplementary Table 3**). However, it is unknown whether the wild-type allele underwent X inactivation in brain tissues as in LCLs and leukocytes from the subjects.

The clinical features of the individuals with SENDA possessing *WDR45* mutations are summarized in **Table 1** (see also the **Supplementary Note**). Subjects 1 and 3 have been described recently[7,8]. These individuals showed psychomotor developmental delay from infancy and severe intellectual disability, while their motor function gradually developed. In adulthood, severe progressive dystonia-parkinsonism and dementia developed. Four of the subjects became bedridden within a few years of onset of cognitive decline. In all subjects, blood concentrations of ceruloplasmin, copper, iron, ferritin and lactate acid were normal. Brain MRI showed T1-weighted signal hyperintensity in the substantia nigra with a central T1-weighted hypointensity band (**Fig. 2a–e**) and T2-weighted signal hypointensity, suggesting iron deposition in the globus pallidus and substantia nigra (**Fig. 2f–h**), which are characteristic of SENDA. In addition, significant cerebral atrophy was found (**Fig. 2i,j**). Substantial differences in the severity of clinical findings were not observed among the five subjects.

WIPI1, WIPI2, WIPI3 and WIPI4, mammalian Atg18 homologs, have an important role in the autophagy pathway[4,5]. Autophagy is the major intracellular degradation system by which cytoplasmic materials are enclosed by double-membrane structures called autophagosomes and subsequently delivered to lysosomes for degradation[9]. More than 30 autophagy-related (ATG) genes have been identified in yeast[10,11], many of which are conserved in higher eukaryotes and are essential for the formation of the autophagosome[10,12]. These factors include subunits of the class III phosphatidylinositol 3-kinase complex, and generation of the lipid phosphatidylinositol 3-phosphate is essential for autophagosome formation. Atg18 in yeast and WIPI subunits in mammals associate with membranes through a phosphoinositide-binding motif (FRRG) within a seven–β propeller structure[13–15]. Atg18 and WIPI proteins also interact with Atg2 and its homologs in yeast and mammalian cells, respectively[16,17]. Autophagic activity in relation to WIPI4 expression was examined using LCLs from the subjects. Immunoblot analysis of WIPI4 showed lower expression in all five subjects compared to unaffected individuals (**Fig. 3a**). Although mutant WIPI4 protein sequence was relatively conserved in subjects 1 and 5, the expression of mutant WIPI4 in both subjects was severely decreased, similar to that of subjects 2, 3 and 4, in whom mutant WIPI4 was truncated. This suggests that all the mutant proteins are structurally unstable and undergo degradation. To examine the effect of the *WDR45* mutations on autophagy, an autophagic flux assay was performed using LCLs. When lysosomal degradation was blocked by the lysosomal inhibitor chloroquine, the amount of LC3-II (the membrane-bound form) was higher than in cells without the inhibitor, as for control LCLs (**Fig. 3b** and **Supplementary Fig. 2**)[18]. The differences in LC3-II amounts between samples with and without chloroquine represent the amount of LC3 on autophagic structures delivered to lysosomes for degradation[18]. In the LCLs from affected subjects, accumulation of LC3-II was observed, even under normal conditions, which was more apparent when autophagy was induced by the mTORC1 inhibitor Torin1 (**Supplementary Fig. 2a–d**). The increase in the LC3-II amount by concomitant chloroquine treatment was significant or tended to be suppressed in the LCLs from affected subjects, suggesting that the autophagic flux was blocked, probably incompletely, at an intermediate step of autophagosome formation (**Fig. 3b** and **Supplementary Fig. 2e**).

Consistent with the immunoblot analysis, immunofluorescence microscopy showed the accumulation of LC3-containing autophagic

Table 1 Clinical features of subjects with SENDA with a *WDR45* mutation

	Subject 1	Subject 2	Subject 3	Subject 4	Subject 5
Age	33 years	28 years	40 years	51 years	33 years
Sex	Female	Female	Female	Female	Female
Mutation	c.439+1G>T	c.516G>C	c.437dupA	c.637C>T	c.1033_1034dupAA
Protein alteration	p.[Gly147Val; Val147_Leu148ins8]	p.Asp174Valfs*29	p.Leu148Alafs*3	p.Gln213*	p.Asn345Lysfs*67
Neurological symptoms					
Current status	Bedridden	Wheelchair	Bedridden	Bedridden	Bedridden
Initial symptom	Psychomotor retardation	Psychomotor retardation	Psychomotor retardation	Psychomotor retardation	Psychomotor retardation
Initial walking	3 years	2 years 7 months	2 years 2 months	1 year 6 months	1 year 6 months
Speech ability	No word	One word	No word	Two-word sentences	Few words
Cognitive dysfunction during childhood	Nonprogressive	Nonprogressive	Nonprogressive	Nonprogressive	Nonprogressive
Start of cognitive decline	26 years	25 years	30 years	24 years	23 years
Period until bedridden after decline	*4 years*	–	*3 years*	*1 year*	*6 years*
Dystonia	+	+	+	+	+
Parkinsonism	Rigidity, akinesia	Rigidity, akinesia	Rigidity	Rigidity	Rigidity, tremor, impairment of postural reflex
Progressive dementia during adulthood	+	+	+	+	+
Psychiatric symptoms	Aggressive behaviors	Aggressive behaviors	None	None	Anxiety
Epileptic seizure	+	+	FS	None	+
Radiological features					
MRI					
Iron deposition	Globus pallidus, substantia nigra	Globus pallidus, substantia nigra	Globus pallidus, substantia nigra	Globus pallidus, substantia nigra	Globus pallidus, substantia nigra
Central band of T1 hypointensity	+	+	+	+	+
Cerebral atrophy	Moderate at 25 years, remarkable at 32 and 33 years	Moderate at 25 and 27 years	Mild at 33 years, remarkable at 39 years	Mild at 27 years, remarkable at 46 years	Remarkable at 33 years
Eye of the tiger sign	–	–	–	–	–
White matter involvement	–	–	–	–	–
Cerebellar atrophy	Mild at 25, 32 and 33 years	Mild at 25 and 27 years	Mild at 33 and 39 years	Mild at 27 and 46 years	Mild at 33 years
CT findings	High density in globus pallidus	Mild high density in substantia nigra	High density in substantia nigra	High density in ventral midbrain	High density in globus pallidus
Neurophysiological examination					
EEG	Bilateral frontal spike	Bilateral frontal spike, low voltage, slow wave	Low voltage	Abnormal	Abnormal
EMG	NE	NE	Dystonic pattern	Normal	NE
VEP	Normal	NE	Prolonged P100 latency	NE	Normal
ABR	Low amplitude, normal latency	NE	No response at 100 dB	NE	NE

FS, febrile seizure; EEG, electroencephalogram; EMG, electromyogram; VEP, visual evoked potential; ABR, auditory brainstem response; NE, not examined.

structures in the LCLs from affected subjects, some of which were abnormally enlarged compared with those observed in control LCLs (**Fig. 3c,d**). Therefore, we examined whether these LC3-positive structures in fact included premature or abnormal autophagic structures. A recent study showed that knockdown of *Wdr45* in rat kidney cells and mutation in *epg-6* (encoding a WIPI4 homolog)

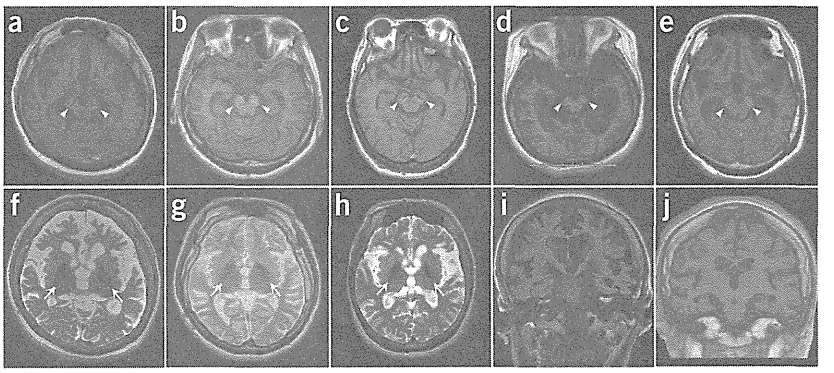

Figure 2 Brain MRIs at 3.0 T and 1.5 T. (**a**–**e**) T1-weighted imaging shows hyperintensity of the substantia nigra with a central band of T1-weighted hypointensity (arrowheads). Images are shown for subject 1 at 33 years (**a**), subject 2 at 25 years (**b**), subject 3 at 39 years (**c**), subject 4 at 46 years (**d**) and subject 5 at 33 years (**e**). (**f**–**h**) T2-weighted imaging shows marked hypointensity of the globus pallidus (arrows), suggesting iron deposition. Cerebral atrophy and mild cerebellar atrophy are also seen. Images are shown for subject 1 (**f**), subject 2 (**g**) and subject 3 (**h**). (**i**,**j**) The fluid attenuated inversion recovery (FLAIR) image of subject 1 (**i**) and the T1-weighted FLAIR coronal image of subject 2 (**j**) also show cerebral atrophy.

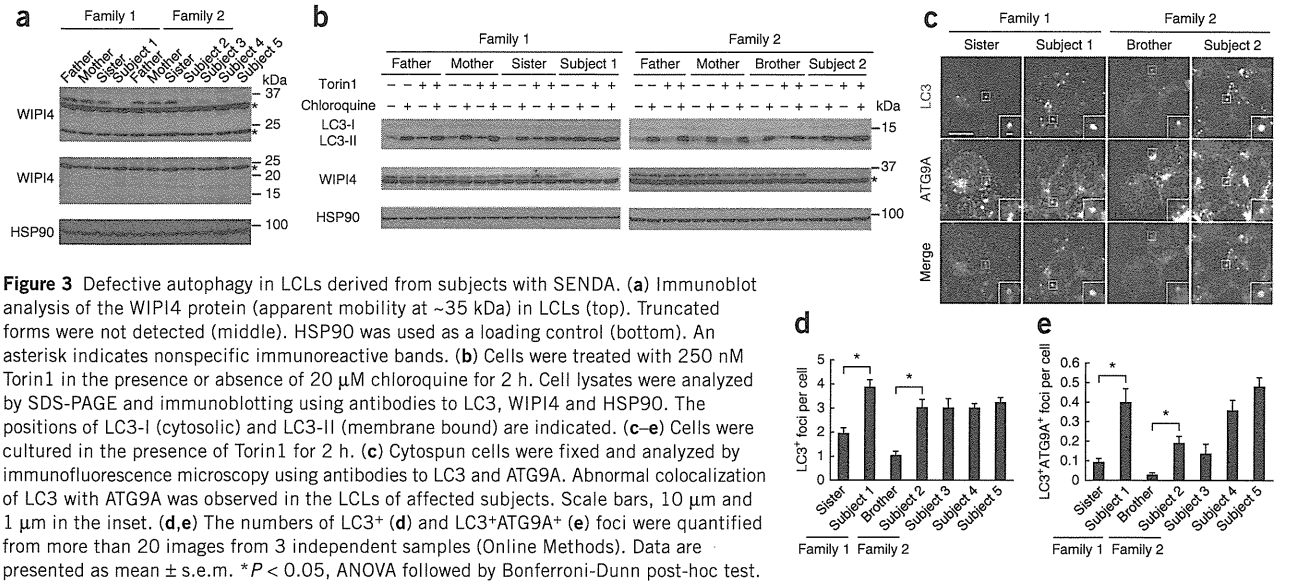

Figure 3 Defective autophagy in LCLs derived from subjects with SENDA. (**a**) Immunoblot analysis of the WIPI4 protein (apparent mobility at ~35 kDa) in LCLs (top). Truncated forms were not detected (middle). HSP90 was used as a loading control (bottom). An asterisk indicates nonspecific immunoreactive bands. (**b**) Cells were treated with 250 nM Torin1 in the presence or absence of 20 μM chloroquine for 2 h. Cell lysates were analyzed by SDS-PAGE and immunoblotting using antibodies to LC3, WIPI4 and HSP90. The positions of LC3-I (cytosolic) and LC3-II (membrane bound) are indicated. (**c**–**e**) Cells were cultured in the presence of Torin1 for 2 h. (**c**) Cytospun cells were fixed and analyzed by immunofluorescence microscopy using antibodies to LC3 and ATG9A. Abnormal colocalization of LC3 with ATG9A was observed in the LCLs of affected subjects. Scale bars, 10 μm and 1 μm in the inset. (**d**,**e**) The numbers of LC3$^+$ (**d**) and LC3$^+$ATG9A$^+$ (**e**) foci were quantified from more than 20 images from 3 independent samples (Online Methods). Data are presented as mean ± s.e.m. $^*P < 0.05$, ANOVA followed by Bonferroni-Dunn post-hoc test.

in *Caenorhabditis elegans* cause accumulation of early autophagic structures[5]. One supposed function of WIPI4 (Epg-6) is to regulate the distribution of ATG9A-marked vesicles[5], which transiently localize to the autophagosome formation site and induce autophagosome formation[19,20]. ATG9A is absent from completed autophagosomes in mammalian cells; therefore, colocalization of ATG9A and LC3 is rare. However, enlarged structures positive for both ATG9A and LC3 accumulated in LCLs from all five subjects (**Fig. 3c,e**), indicating improper autophagosome formation.

The importance of the housekeeping activity of autophagy in neurons, as well as the ubiquitin-proteasome system, has been demonstrated in mice. Mice lacking autophagy in the central nervous system developed progressive motor and behavioral deficits[21,22]. Histologically, inclusion bodies containing polyubiquitinated proteins were observed in neurons, and their size and number increased with age[21,22]. Neuronal cell death was observed in subsets of neurons[21,22], implying that the impairment of autophagy contributes to the pathogenesis of neurodegenerative disorders. Indeed, dysregulation of autophagy has been suggested in various neurodegenerative disorders in humans[23]. In addition, mutations in *PARK2* and *PINK1*, both of which cause familial Parkinson's disease[24,25], impair the selective autophagic degradation of damaged mitochondria, called mitophagy (PARK2, also called Parkin, is recruited to damaged mitochondria in a PINK1-dependent manner)[26,27]. However, a direct link between the core autophagy machinery and human neurodegenerative disorders has not been reported. Here, we showed that mutations in *WDR45*, a core autophagy gene, result in a neurodegenerative disorder. Notably, the autophagy defects were partial, implying that some autophagic activity could be maintained in the neurons of affected subjects. We hypothesize that this might be a possible explanation of why childhood intellectual disability in individuals with SENDA remains static until adulthood, unlike in other forms of NBIA[1–3]. In contrast to heterozygous *WDR45* mutations in females, hemizygous germline mutations in males, leading to the expression of mutant *WDR45* in all cells, possibly cause lethal phenotypes from complete loss of *WDR45* function, as mice defective in autophagy die shortly after birth[28–32]. While this paper was under review, Haack *et al.* reported *WDR45* mutations in 20 subjects, including 3 males, 1 of whom possessed a mutation that was somatic mosaic, supporting the idea that male germline mutations could be lethal[33].

WDR45 is widely expressed in human tissues, with the highest expression found in skeletal muscle[34]. Nevertheless, SENDA phenotypes seem to be limited to the brain. These facts may reflect cell type–dependent differences: autophagy could be more important in neurons (non-dividing, terminally differentiated cells) than in LCLs (rapidly dividing cells). In addition, it is possible that the other WIPI homologs (WIPI1, WIPI2 and WIPI3) could compensate for the deficiency in WIPI4 in a cell type–dependent manner, and the relative contribution of WIPI4 among WIPI factors may be high in neurons.

In conclusion, heterozygous mutations of X-linked *WDR45*, a core autophagy gene, were identified in SENDA, providing direct evidence that an autophagy defect is indeed associated with a neurodegenerative disorder in humans.

URLs. NHLBI Exome Sequencing Project, http://evs.gs.washington.edu/EVS/; Picard, http://picard.sourceforge.net/; SAMtools, http://samtools.sourceforge.net/; dbSNP, http://www.ncbi.nlm.nih.gov/projects/SNP/.

METHODS

Methods and any associated references are available in the online version of the paper.

Accession codes. Reference sequences are available from GenBank for *Homo sapiens WDR45* transcript variant 1 mRNA (NM_007075.3) and WIPI4 isoform 1 (NP_009006.2).

Note: Supplementary information is available in the online version of the paper.

ACKNOWLEDGMENTS

We would like to thank the individuals with SENDA and their families for their participation in this study. We thank M. Shiina and K. Ogata for their helpful comments on the protein structure. This work was supported by research grants from the Ministry of Health, Labour and Welfare (H.S., N. Miyake and N. Matsumoto), the Japan Science and Technology Agency (N. Matsumoto) and the Strategic Research Program for Brain Sciences (N. Matsumoto) and by a Grant-in-Aid for Scientific Research on Innovative Areas (Transcription Cycle) from the Ministry of Education, Culture, Sports, Science and Technology of Japan

(N. Matsumoto), a Grant-in-Aid for Scientific Research from the Japan Society for the Promotion of Science (N. Matsumoto), a Grant-in-Aid for Young Scientists from the Japan Society for the Promotion of Science (H.S. and N. Miyake), the Funding Program for Next-Generation World-Leading Researchers (N. Mizushima) and a grant from the Takeda Science Foundation (N. Miyake, N. Mizushima and N. Matsumoto).

AUTHOR CONTRIBUTIONS

H.S., N. Mizushima and N. Matsumoto designed and directed the study. H.S., T.N., K.M., N. Mizushima and N. Matsumoto wrote the manuscript. K.M., S.K., K.S., E.K.-Y., N.S., H.N., A.H., F.R., S.Y., H.A. and M.K. collected samples and provided the subjects' clinical information. H.S., H.K., K.N., Y.T., M.N. and N. Miyake performed exome sequencing and Sanger sequencing. H.S. and K.N. performed the RNA analysis. Y.K. performed the X-inactivation analysis. T.N. and N. Mizushima analyzed protein expression and autophagic activity.

COMPETING FINANCIAL INTERESTS

The authors declare no competing financial interests.

1. Gregory, A., Polster, B.J. & Hayflick, S.J. Clinical and genetic delineation of neurodegeneration with brain iron accumulation. *J. Med. Genet.* **46**, 73–80 (2009).
2. Kruer, M.C. *et al.* Neuroimaging features of neurodegeneration with brain iron accumulation. *AJNR Am. J. Neuroradiol.* **33**, 407–414 (2012).
3. Schneider, S.A. & Bhatia, K.P. Syndromes of neurodegeneration with brain iron accumulation. *Semin. Pediatr. Neurol.* **19**, 57–66 (2012).
4. Polson, H.E. *et al.* Mammalian Atg18 (WIPI2) localizes to omegasome-anchored phagophores and positively regulates LC3 lipidation. *Autophagy* **6**, 506–522 (2010).
5. Lu, Q. *et al.* The WD40 repeat PtdIns(3)P-binding protein EPG-6 regulates progression of omegasomes to autophagosomes. *Dev. Cell* **21**, 343–357 (2011).
6. Gregory, A. & Hayflick, S.J. Genetics of neurodegeneration with brain iron accumulation. *Curr. Neurol. Neurosci. Rep.* **11**, 254–261 (2011).
7. Kimura, Y. *et al.* MRI, MR spectroscopy, and diffusion tensor imaging findings in patient with static encephalopathy of childhood with neurodegeneration in adulthood (SENDA). *Brain Dev.* published online; doi:10.1016/j.braindev.2012.07.008 (11 August 2012).
8. Kasai-Yoshida, E. *et al.* First video report of static encephalopathy of childhood with neurodegeneration in adulthood. *Mov. Disord.* published online; doi:10.1002/mds.25158 (6 February 2013).
9. Mizushima, N. & Komatsu, M. Autophagy: renovation of cells and tissues. *Cell* **147**, 728–741 (2011).
10. Nakatogawa, H., Suzuki, K., Kamada, Y. & Ohsumi, Y. Dynamics and diversity in autophagy mechanisms: lessons from yeast. *Nat. Rev. Mol. Cell Biol.* **10**, 458–467 (2009).
11. Xie, Z. & Klionsky, D.J. Autophagosome formation: core machinery and adaptations. *Nat. Cell Biol.* **9**, 1102–1109 (2007).
12. Mizushima, N., Yoshimori, T. & Ohsumi, Y. The role of Atg proteins in autophagosome formation. *Annu. Rev. Cell Dev. Biol.* **27**, 107–132 (2011).
13. Baskaran, S., Ragusa, M.J., Boura, E. & Hurley, J.H. Two-site recognition of phosphatidylinositol 3-phosphate by PROPPINs in autophagy. *Mol. Cell* **47**, 339–348 (2012).
14. Krick, R. *et al.* Structural and functional characterization of the two phosphoinositide binding sites of PROPPINs, a β-propeller protein family. *Proc. Natl. Acad. Sci. USA* **109**, E2042–E2049 (2012).
15. Watanabe, Y. *et al.* Structure-based analyses reveal distinct binding sites for Atg2 and phosphoinositides in Atg18. *J. Biol. Chem.* **287**, 31681–31690 (2012).
16. Suzuki, K., Kubota, Y., Sekito, T. & Ohsumi, Y. Hierarchy of Atg proteins in pre-autophagosomal structure organization. *Genes Cells* **12**, 209–218 (2007).
17. Velikkakath, A.K., Nishimura, T., Oita, E., Ishihara, N. & Mizushima, N. Mammalian Atg2 proteins are essential for autophagosome formation and important for regulation of size and distribution of lipid droplets. *Mol. Biol. Cell* **23**, 896–909 (2012).
18. Mizushima, N., Yoshimori, T. & Levine, B. Methods in mammalian autophagy research. *Cell* **140**, 313–326 (2010).
19. Itakura, E., Kishi-Itakura, C., Koyama-Honda, I. & Mizushima, N. Structures containing Atg9A and the ULK1 complex independently target depolarized mitochondria at initial stages of Parkin-mediated mitophagy. *J. Cell Sci.* **125**, 1488–1499 (2012).
20. Orsi, A. *et al.* Dynamic and transient interactions of Atg9 with autophagosomes, but not membrane integration, are required for autophagy. *Mol. Biol. Cell* **23**, 1860–1873 (2012).
21. Hara, T. *et al.* Suppression of basal autophagy in neural cells causes neurodegenerative disease in mice. *Nature* **441**, 885–889 (2006).
22. Komatsu, M. *et al.* Loss of autophagy in the central nervous system causes neurodegeneration in mice. *Nature* **441**, 880–884 (2006).
23. Menzies, F.M., Moreau, K. & Rubinsztein, D.C. Protein misfolding disorders and macroautophagy. *Curr. Opin. Cell Biol.* **23**, 190–197 (2011).
24. Valente, E.M. *et al.* Hereditary early-onset Parkinson's disease caused by mutations in *PINK1*. *Science* **304**, 1158–1160 (2004).
25. Kitada, T. *et al.* Mutations in the *parkin* gene cause autosomal recessive juvenile parkinsonism. *Nature* **392**, 605–608 (1998).
26. Youle, R.J. & van der Bliek, A.M. Mitochondrial fission, fusion, and stress. *Science* **337**, 1062–1065 (2012).
27. Youle, R.J. & Narendra, D.P. Mechanisms of mitophagy. *Nat. Rev. Mol. Cell Biol.* **12**, 9–14 (2011).
28. Kuma, A. *et al.* The role of autophagy during the early neonatal starvation period. *Nature* **432**, 1032–1036 (2004).
29. Saitoh, T. *et al.* Loss of the autophagy protein Atg16L1 enhances endotoxin-induced IL-1β production. *Nature* **456**, 264–268 (2008).
30. Saitoh, T. *et al.* Atg9a controls dsDNA-driven dynamic translocation of STING and the innate immune response. *Proc. Natl. Acad. Sci. USA* **106**, 20842–20846 (2009).
31. Sou, Y.S. *et al.* The Atg8 conjugation system is indispensable for proper development of autophagic isolation membranes in mice. *Mol. Biol. Cell* **19**, 4762–4775 (2008).
32. Komatsu, M. *et al.* Impairment of starvation-induced and constitutive autophagy in *Atg7*-deficient mice. *J. Cell Biol.* **169**, 425–434 (2005).
33. Haack, T.B. *et al.* Exome sequencing reveals *de novo WDR45* mutations causing a phenotypically distinct, X-linked dominant form of NBIA. *Am. J. Hum. Genet.* **91**, 1144–1149 (2012).
34. Proikas-Cezanne, T. *et al.* WIPI-1α (WIPI49), a member of the novel 7-bladed WIPI protein family, is aberrantly expressed in human cancer and is linked to starvation-induced autophagy. *Oncogene* **23**, 9314–9325 (2004).

ONLINE METHODS

Subjects. We analyzed five Japanese individuals with SENDA. Diagnosis was made on the basis of clinical features, including psychomotor retardation at early childhood that was static for decades and severe progressive dystonia-parkinsonism and dementia after several decades, as well as characteristic findings on brain MRI scans. Genomic DNA was isolated from blood leukocytes according to standard protocols. The Institutional Review Board of Yokohama City University approved the experimental protocols. Informed consent was obtained for all individuals included in this study in agreement with the requirements of Japanese regulations. Clinical information on the subjects with a *WDR45* mutation is presented in **Table 1** and in the **Supplementary Note**.

Mutation screening. Mutation screening of exons 3–12 covering the *WDR45* coding region (of transcript variant 1, GenBank accession NM_007075.3) was performed by direct sequencing. PCR was performed in a 20-μl mixture containing 1 μl of genomic DNA, 1× PCR Buffer for KOD FX NEO, 0.4 mM of each dNTP, 0.3 μM of each primer and 0.4 U of KOD FX NEO polymerase (Toyobo). Details on PCR conditions and primer sequences are given in **Supplementary Table 4**.

Exome sequencing. Genomic DNA was captured using the SureSelect Human All Exon v4 kit (51 Mb; Agilent Technologies) and sequenced with four samples per lane on an Illumina HiSeq2000 with 101-bp paired-end reads. Image analysis and base calling were performed by sequence control software real-time analysis and CASAVA software v1.8 (Illumina). Reads were aligned to GRCh37 with Novoalign (Novocraft Technologies). Duplicate reads were marked using Picard (see URLs) and excluded from downstream analysis. After merging the BAM files of all members in each family using SAMtools, local realignments around indels and base quality score recalibration were performed with the Genome Analysis Toolkit (GATK)[35]. Single-nucleotide variants and small indels were identified using the GATK UnifiedGenotyper and filtered according to the Broad Institute's best-practice guidelines (version 3). Variants registered in dbSNP135, which were not flagged as clinically associated, were excluded. Variants that passed the filters were annotated using ANNOVAR[36].

RNA analysis. LCLs were established from five affected subjects and their family members. RT-PCR using total RNA extracted from LCLs was performed as previously described[37]. Briefly, 4 μg of total RNA extracted with an RNeasy Plus Mini kit (Qiagen) was subjected to reverse transcription, and 2 μl of cDNA was used for PCR. Details on primer sequences and PCR conditions are given in **Supplementary Table 4**. PCR products were electrophoresed in a 10% polyacrylamide gel and sequenced.

X-inactivation analysis. The X-inactivation pattern was studied using the human androgen receptor (HUMARA) assay and a fragile X mental retardation (*FRAXA*) locus methylation assay as previously described[38–40]. Briefly, genomic DNA from the subjects, a control male and a control female was digested with two methylation-sensitive enzymes, HpaII and HhaI. Details on PCR conditions and primer sequences are given in **Supplementary Table 4**. Fluorescently labeled products were analyzed on an ABI PRISM 3500 Genetic Analyzer with GeneMapper Software version 4.0 (Applied Biosystems). X-inactivation ratios of less than or equal to 80:20 were considered to represent a random pattern, ratios greater than 80:20 were considered to represent a skewed pattern, and ratios greater than 90:10 were considered to represent a markedly skewed pattern[38].

Cell culture. LCLs were cultured in RPMI 1640 supplemented with 10% FBS, L-glutamine, tylosin and antibiotic-antimycotic solution in a 5% CO_2 incubator.

Immunoblotting. An affinity-purified rabbit polyclonal antibody against WIPI4 peptide antigen (CFPDNPRKLFEFDTRDNP, amino acids 129–145) was generated by Medical & Biological Laboratories. The specificity of the antibody was tested using lysate from HeLa cells in which *WDR45* was knocked down. For immunoblot analysis, cells were lysed with lysis buffer (50 mM Tris-HCl, pH 7.5, 150 mM NaCl, 1 mM EDTA, 1% Triton X-100, 1 mM phenylmethanesulfonyl fluoride and a protease inhibitor cocktail (Complete EDTA-free protease inhibitor, Roche)). Cell lysates were clarified by centrifugation at 12,000*g* for 20 min and analyzed by SDS-PAGE and immunoblotting using antibodies to WIPI4, LC3 (ref. 41) and HSP90 (BD Transduction Laboratories, 610418). Signal intensities were analyzed using a LAS-3000 mini imaging analyzer and Multi Gauge software version 3.0 (Fujifilm). Contrast and brightness adjustments were applied to the images using Photoshop 7.0.1 (Adobe Systems).

Fluorescence microscopy. LCLs were spun onto a glass slide at 500 RPM (28*g*) for 1 min in a Shandon Cytospin 4 cytofuge (Thermo Electron). Cells were fixed with 4% paraformaldehyde, permeabilized using 50 μg/ml digitonin and then stained with antibodies to LC3 (clone 1703, Cosmo Bio) and Atg9A[19]. Cells were observed with a confocal laser microscope (FV1000D IX81, Olympus) using a 60× PlanApoN oil immersion lens (1.42 numerical aperture (N.A.), Olympus). For final output, images were processed using Adobe Photoshop 7.0.1 software. The number of staining foci was determined as follows: foci were extracted using the top hat operation (parameter of 300 × 300 pixel area), and a binary image was created. Small foci (with an area of less than 10 × 10 pixels) were removed using an open operation. The number of foci was counted using the integrated morphometry analysis program. False foci were removed by comparison with the original image.

Statistical analysis. Differences were analyzed statistically using unpaired *t* tests or analysis of variance (ANOVA) with a Bonferroni-Dunn post-hoc test.

35. DePristo, M.A. *et al.* A framework for variation discovery and genotyping using next-generation DNA sequencing data. *Nat. Genet.* **43**, 491–498 (2011).
36. Wang, K., Li, M. & Hakonarson, H. ANNOVAR: functional annotation of genetic variants from high-throughput sequencing data. *Nucleic Acids Res.* **38**, e164 (2010).
37. Saitsu, H. *et al. STXBP1* mutations in early infantile epileptic encephalopathy with suppression-burst pattern. *Epilepsia* **51**, 2397–2405 (2010).
38. Kondo, Y. *et al.* A family of oculofaciocardiodental syndrome (OFCD) with a novel *BCOR* mutation and genomic rearrangements involving *NHS*. *J. Hum. Genet.* **57**, 197–201 (2012).
39. Allen, R.C., Zoghbi, H.Y., Moseley, A.B., Rosenblatt, H.M. & Belmont, J.W. Methylation of HpaII and HhaI sites near the polymorphic CAG repeat in the human androgen-receptor gene correlates with X chromosome inactivation. *Am. J. Hum. Genet.* **51**, 1229–1239 (1992).
40. Carrel, L. & Willard, H.F. An assay for X inactivation based on differential methylation at the fragile X locus, *FMR1*. *Am. J. Med. Genet.* **64**, 27–30 (1996).
41. Hosokawa, N., Hara, Y. & Mizushima, N. Generation of cell lines with tetracycline-regulated autophagy and a role for autophagy in controlling cell size. *FEBS Lett.* **580**, 2623–2629 (2006).

PLOS ONE

Common and Distinct Clinical Features in Adult Patients with Anti-Aminoacyl-tRNA Synthetase Antibodies: Heterogeneity within the Syndrome

Yasuhito Hamaguchi[1], Manabu Fujimoto[1]*, Takashi Matsushita[1], Kenzo Kaji[1], Kazuhiro Komura[1], Minoru Hasegawa[1], Masanari Kodera[2], Eiji Muroi[3], Keita Fujikawa[4], Mariko Seishima[5], Hidehiro Yamada[6], Ryo Yamada[7], Shinichi Sato[8], Kazuhiko Takehara[1], Masataka Kuwana[9]

1 Department of Dermatology, Kanazawa University Graduate School of Medical Science, Kanazawa, Japan, **2** Department of Dermatology, Social Insurance Chukyo Hospital, Nagoya, Japan, **3** Department of Dermatology, Nagasaki University Graduate School of Biomedical Sciences, Nagasaki, Japan, **4** Unit of Translational Medicine, Department of Immunology and Rheumatology, Nagasaki University Graduate School of Biomedical Sciences, Nagasaki, Japan, **5** Department of Dermatology, Ogaki Municipal Hospital, Ogaki, Japan, **6** Division of Rheumatology, Department of Internal Medicine, and Allergy, St. Marianna University, Kawasaki, Japan, **7** Center for Genomic Medicine, Graduate School of Medicine, Kyoto University, Kyoto, Japan, **8** Department of Dermatology, Faculty of Medicine, University of Tokyo, Tokyo, Japan, **9** Division of Rheumatology, Department of Internal Medicine, Keio University School of Medicine, Tokyo, Japan

Abstract

Objective: To identify similarities and differences in the clinical features of adult Japanese patients with individual anti-aminoacyl-tRNA synthetase antibodies (anti-ARS Abs).

Methods: This was a retrospective analysis of 166 adult Japanese patients with anti-ARS Abs detected by immunoprecipitation assays. These patients had visited Kanazawa University Hospital or collaborating medical centers from 2003 to 2009.

Results: Anti-ARS Ab specificity included anti-Jo-1 (36%), anti-EJ (23%), anti-PL-7 (18%), anti-PL-12 (11%), anti-KS (8%), and anti-OJ (5%). These anti-ARS Abs were mutually exclusive, except for one serum Ab that had both anti-PL-7 and PL-12 reactivity. Myositis was closely associated with anti-Jo-1, anti-EJ, and anti-PL-7, while interstitial lung disease (ILD) was correlated with all 6 anti-ARS Abs. Dermatomyositis (DM)-specific skin manifestations (heliotrope rash and Gottron's sign) were frequently observed in patients with anti-Jo-1, anti-EJ, anti-PL-7, and anti-PL-12. Therefore, most clinical diagnoses were polymyositis or DM for anti-Jo-1, anti-EJ, and anti-PL-7; clinically amyopathic DM or ILD for anti-PL-12; and ILD for anti-KS and anti-OJ. Patients with anti-Jo-1, anti-EJ, and anti-PL-7 developed myositis later if they had ILD alone at the time of disease onset, and most patients with anti-ARS Abs eventually developed ILD if they did not have ILD at disease onset.

Conclusion: Patients with anti-ARS Abs are relatively homogeneous. However, the distribution and timing of myositis, ILD, and rashes differ among patients with individual anti-ARS Abs. Thus, identification of individual anti-ARS Abs is beneficial to define this rather homogeneous subset and to predict clinical outcomes within the "anti-synthetase syndrome."

Citation: Hamaguchi Y, Fujimoto M, Matsushita T, Kaji K, Komura K, et al. (2013) Common and Distinct Clinical Features in Adult Patients with Anti-Aminoacyl-tRNA Synthetase Antibodies: Heterogeneity within the Syndrome. PLoS ONE 8(4): e60442. doi:10.1371/journal.pone.0060442

Editor: Frederick Miller, National Institutes of Health, United States of America

Received November 13, 2012; **Accepted** February 27, 2013; **Published** April 3, 2013

Funding: This work was supported by a research grant on intractable diseases from the Ministry of Health, Labor and Welfare of Japan (to Manabu Fujimoto). The funders had no role in study design, data collection and analysis, decision to publish, or preparation of the manuscript.

Competing Interests: The authors have declared that no competing interests exist.

* E-mail: fujimoto-m@umin.ac.jp

Introduction

The presence of autoantibodies (Abs) is one of the hallmarks of connective tissue diseases, such as systemic lupus erythematosus (SLE), systemic sclerosis (SSc), and idiopathic inflammatory myopathy. In particular, a variety of serum Abs is found in patients with idiopathic inflammatory myopathies, including polymyositis (PM) and dermatomyositis (DM) [1,2]. It is clinically of considerable importance to identify Abs in patients with PM/DM, because each Ab is closely associated with certain clinical features [3]. For example, anti-Mi-2 is associated with classic DM without interstitial lung disease (ILD) or malignancy and with good response to treatment [4–6]; anti-155/140 is associated with malignancy-associated or juvenile DM [7–10]; and anti-CADM-140/MDA5 is associated with clinically amyopathic DM (CADM) and rapidly progressive-ILD (RP-ILD) that results in poor prognosis [11,12]. Abs reactive with aminoacyl-tRNA synthetases (ARS) are also representative Abs that are detected in patients with PM/DM. Eight anti-ARS Abs have been described: anti-histidyl (anti-Jo-1), anti-threonyl (anti-PL-7), anti-alanyl (anti-PL-12), anti-glycyl (anti-EJ), anti-isoleucyl (anti-OJ), anti-asparaginyl (anti-KS), anti-phenylalanyl (anti-Zo), and anti-tyrosyl (anti-Ha) tRNAs [13–20]. Based on a unique combination of clinical features commonly observed in patients with anti-ARS Abs, Targoff proposed a

disease entity termed "anti-synthetase syndrome," which is characterized by myositis, ILD, fever, Raynaud's phenomenon, arthritis, and mechanic's hands [21]. Although anti-synthetase syndrome has common clinical manifestations, further observations have distinguished some differences in clinical features associated with individual anti-ARS Abs [22]. For example, it has been reported that anti-Jo-1 Abs are closely associated with myositis [14,17], whereas patients with anti-KS are more likely to have ILD without clinical evidence of myositis [18,23]. On the other hand, Sato *et al* previously reported that the presence of anti-PL-7 is closely associated with PM/DM-SSc overlap as well as ILD in Japanese patients [24].

This is a large comprehensive study to focus on the clinical and laboratory features in adult patients with anti-ARS Abs for the investigation of similarities and differences in these anti-ARS Abs. The results of this study indicate that anti-ARS Abs share several clinical features, but also have some considerable differences. Thus, identification of each anti-ARS Ab is beneficial to define this rather homogeneous subset of patients and to predict clinical outcomes.

Patients and Methods

Ethics Statement

Ethical approval for the study was obtained from the individual institutional review boards (Kanazawa University, Keio University, Nagasaki University, St. Marianna University, Social Insurance Chukyo Hospital, and Ogaki Municipal Hospital) and all sera were collected after the subjects gave their written informed consent.

Patients and Sera

Serum samples were obtained from Japanese patients with autoimmune diseases or related disorders who had visited Kanazawa University Hospital or collaborating medical centers from 2003 to 2009. In total, 3164 samples (from 478 patients with DM/PM, 498 with SSc, 183 with ILD alone, 376 with SLE, 102 with mixed connective tissue disease, 398 with Sjogren's syndrome, and 1129 with rheumatoid arthritis) were screened by immunoprecipitation (IP) assay for the detection of antinuclear or anticytoplasmic antibodies. These patients were referred mainly by rheumatologists, dermatologists, or pulmonologists. PM and classic DM were defined by fulfillment of the Bohan and Peter criteria for definite or probable diagnoses [25]. DM was distinguished from PM based on the presence of heliotrope rash or Gottron's lesions (Gottron's papules and/or Gottron's sign). The diagnosis of CADM was based on the criteria proposed by Sontheimer [26], as follows: clinical skin manifestations typical of DM but minimal or no clinical features of myositis for >2 years after the onset of skin manifestations. All patients with SLE or SSc fulfilled the American College of Rheumatology criteria [27,28]. PM/DM-overlap was diagnosed by the coexistence of SLE and/or SSc in addition to PM or DM. "ILD alone" was defined by the presence of ILD without fulfillment of any of the criteria for PM, DM, CADM, SLE, or SSc. Patients with ILD alone were examined for potential coexistence of myositis by evaluating muscle weakness and serum muscle enzyme levels including creatine kinase (CK) and aldolase during follow-up, while those without ILD were examined for potential coexistence of ILD by examining dyspneic symptoms and chest radiograph and/or high-resolution computed tomography (HRCT) at every 3 to 6 months.

Clinical information was collected retrospectively for all patients with anti-ARS Abs by reviewing their clinical charts. Initial manifestations were defined as the clinical presentation at the first clinic visit. Patients who had at least one of the following symptoms: symmetrical proximal muscle weakness, muscle pain, or elevated levels of myogenic enzymes, underwent electromyogram, MRI, and/or muscle biopsy for confirmation of the presence of myositis. Patients were diagnosed with myositis if at least one of these confirmatory examinations showed findings compatible with inflammatory myopathy: a myogenic pattern on electromyogram [25], muscular edema on T2-weighted images with fat suppression on MRI [29], or necrosis, regeneration, and some atrophy of muscle fibers and inflammatory cell infiltration on muscle biopsy [25]. Patients were diagnosed as having ILD according to the images on chest HRCT. RP-ILD was defined as progressive dyspnea and progressive hypoxemia with a worsening of interstitial changes on the chest images within 1 month from the onset of respiratory manifestations [11]. Internal and hematologic malignancies in anti-ARS-positive patients was defined if the malignant disease was diagnosed concurrently with or within 3 years after diagnosis of anti-synthetase syndrome or if a preceding malignant disease occurred within 3 years before diagnosis of anti-synthetase syndrome [4]. Sjögren's syndrome was defined in accordance with the revised European criteria [30].

IP Assays

Protein IP assays were carried out with extracts of the leukemia cell line, K562 [11]. A total of 10 μl of the patient's serum was bound to 2 mg protein-A Sepharose beads (Amersham Biosciences, Piscataway, NJ) in 500 μl of IP buffer (10 mM Tris-HCl, pH 8.0, 50 mM NaCl, 0.1% Nonidet P-40), incubated for 2 h at 4°C, and then washed five times with IP buffer. Ab-coated Sepharose beads were mixed with 100 μl ^{35}S-methionine-labelled K562 cell extracts derived from 10^6 cells and rotated at 4°C for 2 h. After five washes, the beads were resuspended in sodium dodecyl sulphate (SDS) sample buffer and the polypeptides were fractionated by 7.5% SDS-polyacrylamide gel electrophoresis (PAGE) followed by autoradiography. For the analysis of RNA, immunoprecipitated RNA was detected in 8% urea-PAGE from a cell extract obtained from 3×10^6 non-radiolabeled K562 cells by phenol/chloroform, visualized by silver staining [31]. Each anti-ARS Ab was considered positive if serum samples produced precipitin lines with immunological identity to reference sera by both protein and RNA IP [32]. Anti-Ro Ab and anti-La Ab were detected by IP assays as well. Serum was considered positive for anti-Ro Ab if at least one of the Y1–Y5 RNAs was detected by RNA IP and the 60 kDa protein was detected by protein IP; serum was considered positive for anti-La Ab if RNAs contained in the 7S and 5.8S lesions were detected by RNA IP and the 48 kDa protein was detected by protein IP.

Immunofluorescence

Indirect immunofluorescence tests were carried out with slides of monolayer HEp-2 cells (Medical & Biological Laboratories [MBL], Nagoya, Japan) as substrate [33]. Anticentromere antibody was considered positive if serum diluted at 1:40 produced a characteristic staining pattern on HEp-2 cells as well as on commercially prepared HeLa cell chromosomal spreads (MBL) [34].

Statistical Analysis

Frequencies among all six anti-ARS-positive subgroups were compared with a chi-square test. If the overall P value was less than 0.05, pairwise comparisons were performed with a chi-square test with Yates' correction where appropriate. Continuous variables confirmed to be normally distributed were shown as mean and SD, and their comparisons among groups were carried